Article (refereed) - postprint

Gilbert, Mark A.; Gaffney, Eamonn A.; Bullock, James M.; White, Steven M. 2014. **Spreading speeds for plant populations in landscapes with low environmental variation**.

# Spreading Speeds for Plant Populations in Landscapes with Low Environmental Variation

Mark A. Gilbert[a,b,*], Steven M. White[a,b], James M. Bullock[b], Eamonn A. Gaffney[a]

[a] *Wolfson Centre for Mathematical Biology, Mathematical Institute, Radcliffe Observatory Quarter, Woodstock Road, Oxford, Oxfordshire, OX2 6GG, UK*
[b] *Centre for Ecology & Hydrology, Benson Lane, Wallingford, Oxfordshire, OX10 8BB, UK*

**Abstract**

Characterising the spread of biological populations is crucial in responding to both biological invasions and the shifting of habitat under climate change. Spreading speeds can be studied through mathematical models such as the discrete-time integro-difference equation (IDE) framework. The usual approach in implementing IDE models has been to ignore spatial variation in the demographic and dispersal parameters and to assume that these are spatially homogeneous. On the other hand, real landscapes are rarely spatially uniform with environmental variation being very important in determining biological spread. This raises the question of under what circumstances spatial structure need not be modelled explicitly. Recent work has shown that spatial variation can be ignored in models in the specific case where the scale of landscape variation is much smaller than the spreading population's dispersal scale. We consider more general types of landscape, where the spatial scales of environmental variation are arbitrarily large, but the maximum change in environmental parameters is relatively small. We find that the difference between the wave-speeds of populations spreading in a spatially structured periodic landscape and its homogenisation is, in general, proportional to $\epsilon^2$, where $\epsilon$ governs the degree of environmental variation. For stochastically generated landscapes we numerically demonstrate that the error decays faster than $\epsilon$. In both cases, this means that for sufficiently small $\epsilon$, the homogeneous approximation is better than might be expected. Hence, in many situations, the precise details of the landscape can be ignored in favour of spatially homogeneous parameters. This means that field ecologists can use the homogeneous IDE as a relatively simple modelling tool - in terms of both measuring parameter values and doing the modelling itself. However, as $\epsilon$ increases, this homogeneous approximation loses its accuracy. The change in wave-speed due to the extrinisic (landscape) variation can be positive or negative, which is in contrast to the reduction in wave-speed caused by intrinsic stochasticity. To deal with the loss of accuracy as $\epsilon$ increases, we formulate a second order approximation to the wave-speed for periodic landscapes and compare both approximations against the results of numerical simulation and show that they are both accurate for the range of landscapes considered.

*Corresponding author.
*Email addresses:* gilbert@maths.ox.ac.uk (Mark A. Gilbert), smwhit@ceh.ac.uk (Steven M. White), jmbul@ceh.ac.uk (James M. Bullock), gaffney@maths.ox.ac.uk (Eamonn A. Gaffney)

## 1. Introduction

Understanding the changing spatial distributions of plant populations is of utmost importance to ecologists, environmental managers, conservationists [1] and agronomists [2]. This is due to both the sizeable environmental and economic impacts of biological invasions [2, 3, 4, 5] and the need for species to keep pace with shifting habitat if they are to survive the effects of climate change [6, 7, 8]. Developing the understanding of spatial spread through mathematical modelling should enhance our ability to manage invasive species and the ecological effects of climate change (e.g. [9]).

Extrinisic (landscape) and intrinsic (individual) variation have both been found to be important factors in determining whether a population spreads and its spread rate. Lewis et al [10] found that the effect of intrinisic variation is to reduce a population's spreading ability and speed. In contrast, while landscape structure is a decisive factor in determining a population's spreading ability and speed [7, 11], the precise way it affects spread is more complicated. Mathematical models of population spread have addressed landscape structure in two ways (e.g. [12, 13]). At one extreme, models have been developed to represent fragmented landscapes [14] while at the other, many researchers have treated landscapes as homogeneous [15, 16, 17, 18]. One might expect that neglecting to incorporate the landscape structure explicitly would result in inaccurate predictions of spread, however homogeneous approximations have been relatively successful when compared with real data, for example [19, 20]. Here, we will address the question of under what circumstances the details of landscape structure can be ignored, and when they must be taken into account if accurate predictions are to be made.

We use an Integrodifference Equation (IDE) framework [21] to model spreading populations. IDEs treat population growth and dispersal as separate sequential phases in an (e.g. annual) cycle and have been widely used to study population spread, especially in plants [19, 8, 22, 23, 24]. IDEs can incorporate stage-structured matrix population models [18] and any dispersal pattern that can be formulated as a *dispersal kernel*, the distribution of displacements of individuals from their original position, or (for juveniles) the position of their parent. Landscape heterogeneity can be introduced to the model in terms of spatially heterogeneous parameters in the dispersal kernel or the population projection matrix.

The general stage-structured, spatially heterogeneous IDE [18] in one spatial dimension relates the continuous population distribution at time $t+1$ with the vector valued stage-structured distribution $\mathbf{u}^t(x)$ at time $t$ and location $x \in \mathbb{R}$, via

$$\mathbf{u}^{t+1}(x) = \int_{-\infty}^{\infty} \left[\mathbf{K}(x-y,y) \circ \mathbf{B}\left(\mathbf{u}^t(y),y\right)\right] \mathbf{u}^t(y)\mathrm{d}y \ , \tag{1}$$

where $\circ$ denotes the Hadamard (elementwise) product of two matrices [18]. This relation is non-dimensional

in that we do not give scales or units to length, population density or time, with the analysis applicable to all choices of length and time scales. In the integrand $\mathbf{B}\left(\mathbf{u}^t(y), y\right)$ is the *population projection matrix*, with its $(i,j)$-th entry being the ratio of the number of individuals in stage $j$ after the growth phase and the number individuals in stage $i$ at time $t$ (at location $y$). $\mathbf{K}(x-y,y)$ is the matrix of dispersal kernels $K_{i,j}(x-y,y)$ for individuals which transitioned from stage $i$ to stage $j$ in the growth phase. It is necessary to consider the dispersal pattern of individuals transitioning between each (permitted) pair of demographic stages separately, as the stage of the individual or, in the case of juveniles, its parent before the growth phase will often affect the individual's dispersal behaviour. For example, for plants with wind dispersed seeds, the mean dispersal distance of a seed/new juvenile will depend on the seed release height of its parent and therefore on its parent's demographic stage (e.g. [25]).

The long-term behaviour and spreading speeds of solutions to (1) can be studied through numerical simulation. However, analytical expressions for the persistence and spreading speed are very useful in understanding parameter dependencies. Additionally, their calculation is much less computationally expensive than numerical simulation, so allowing extensive parameter sweeps when calculating the effects of different factors on the speed at which the population propagates, the *wave-speed*.

For spatially homogeneous IDEs with no Allee effect we can find a simple expression for the wave-speed as long as this wave-speed is *linearly determined* and constant (rather than accelerating). These are guaranteed by the conditions that:

I. The demographic matrix $\mathbf{B}$ is either positive, or nonnegative and primitive.

II. Each element of the matrix of kernels $K_{i,j}(z,y)$ have moment generating functions in $z$, i.e. the dispersal kernel from each point $y$ between each pair of demographic stages is *exponentially bounded*. This condition ensures that solutions have a constant wave-speed and do not accelerate [17].

III. The constant zero population state is globally unstable, i.e. any initial arbitrarily small population, located anywhere, will invade and tend towards the non-zero equilibrium of the habitat as $t \to \infty$.

IV. Increased population density reduces the effect of the demographic matrix on any population distribution, i.e.

$$\mathbf{B}\left(\mathbf{0}, y\right)\mathbf{u} \geq \mathbf{B}\left(\mathbf{u}, y\right)\mathbf{u} \quad \text{for all } \mathbf{u} \in \mathbb{R}^M$$

where the inequality is evaluated elementwise and $M$ is the number of demographic stages.

We will assume these standard [18] conditions for the analysis in the remainder of the paper. Where the growth and dispersal parameters are independent of spatial location and the above conditions are satisfied, the wave-speed is given by

$$\hat{c} = \min_{s>0} \left( \frac{1}{s} \log \left( \rho(s) \right) \right) \tag{2}$$

where $\rho(s)$ is the principal (largest in absolute value) eigenvalue of the operator

$$\mathbf{H}(s) = \int_{-\infty}^{\infty} \left[ \mathbf{K}(z) \circ \mathbf{A} \right] \mathrm{e}^{sz} \mathrm{d}z \ . \tag{3}$$

For spatially heterogeneous IDEs, no equivalent expression exists. This has led to the development of several analytical approximations for the wave-speed in different scenarios and asymptotic limits. Due to their relative tractability, these analyses have focused on *periodic landscapes* of alternate ('good' and 'bad') patches with different values for the growth and dispersal parameters. Kawasaki and Shigesada (2007) developed approximations for cases when dispersal is given by the Laplace (exponential) kernel [26]. Other researchers have developed approximations applicable to any exponentially bounded kernel, but where certain parameters in the model must be related to each other by a small parameter $\epsilon \ll 1$ (with smaller $\epsilon$ giving a greater degree of accuracy). Dewhirst and Lutscher (2009) [13] considered landscapes where the period of the landscape is much smaller than the scale of dispersal. They used *averaging techniques*, replacing the spatially heterogeneous parameters with their spatial homogenisation (average) and using the results for homogeneous landscapes. Gilbert et al (2014) [14] found approximations for periodic landscapes in which the spatial scale of the good patches is much smaller than the scale of dispersal and the demographic rates in the good patches are much greater than those in the bad patches.

The existing approximations give accurate results (when compared with numerical simulation) for spreading speeds of populations with a particular dispersal kernel or in the relevant asymptotic limit. In contrast to previous studies, in this paper we will derive results for landscapes with low environmental variation, in which the environmentally driven variation in demographic parameters relative to the mean, $\epsilon$, is small (i.e. $\epsilon \ll 1$). For example, fecundity may be slightly higher than the mean in some locations and slightly lower in others. Low environmental variation in population measures and environmental conditions within landscapes has been documented by several authors [27, 28]. For example, Janišová et al (2012) [29] measured the demographic matrices of the endangered flowering plant *Tephroseris longifolia* across five locations in a grassland/scrub landscape in the Czech Republic and Slovakia and found their principal eigenvalues to vary between 1.25 and 2.04 (a maximum relative variation of 0.31 from the mean). Generally, one might expect a population to encounter low environmental variation when spreading across a single continuous habitat, such as prairie, boreal forest, or regions converted to arable agriculture.

We show that when the environmental variation coefficient $\epsilon$ is small, the asymptotic wave-speeds $\hat{c}(\epsilon)$ and $\hat{c}(0)$ corresponding to the heterogeneous landscape and its homogenisation differ by an additive factor of size $\epsilon^2$, providing a justification for studying the homogenisations of landscapes with low environmental

variation. We will also derive a *second order* approximation for the wave-speed in these weakly heterogeneous landscapes which will act as a better approximation for larger $\epsilon$. Using numerical simulation, we will show that both the homogeneous and second order approximations are accurate for $\epsilon < 0.3$, with the second order approximation dramatically reducing the error. We will also explore the relationship between $\epsilon$ and the wave-speed in a non-periodic (stochastically generated) landscape, and will find a similar lack of sensitivity to $\epsilon$ for sufficiently small values of $\epsilon$. For both periodic and stochastically generated landscapes, we find that extrinsic environmental variation can both speed up and slow down invasions, with the specific effect having complex dependencies on the difference between landscape variation and dispersal scales, the mean demographic/dispersal rates and on the dispersal kernel. This is in contrast to the effects of intrinsic stochasticity studied by Lewis et al [10] which were found to always slow down spread. How small $\epsilon$ needs to be in practice for the homogeneous approximation to work will depend on the average parameters of the organism and the landscape itself and will therefore be explored.

## 2. Method

In this section, we will show that, for periodic landscapes, the error of the homogeneous approximation is proportional to $\epsilon^2$ and therefore that the homogeneous approximation is accurate for sufficiently small $\epsilon$ (§2.1). We will then derive a second order approximation, which incorporates the second non-zero term in the eigenvalue of the dispersion relation (§2.2), and finally, will discuss the extension of the periodic results in §2.1-2 to non-periodic landscapes (§2.3).

### *2.1. Accuracy of the Homogeneous Approximation*

We consider the wave-speed solutions of equations of the form (1) where the initial conditions $\mathbf{u}^0(x)$ are non-zero only on some closed interval $[x_{\min}, x_{\max}]$ where $x_{\min}, x_{\max}$ are finite (mathematically, they have *compact support*). The landscape parameters are periodic and *weakly heterogeneous*, i.e. each dispersal and growth parameter exhibits only $\mathrm{O}(\epsilon)$ proportional variation from its spatial mean, where $\epsilon \ll 1$ (see Condition V).

To demonstrate analytically that there is only an $\mathrm{O}(\epsilon^2)$ difference in asymptotic wave-speed between solutions of this model and solutions of the spatially averaged homogeneous model (where the growth and dispersal parameters are constant and given by the spatial averages of the parameters used in (1)) we require that the IDE satisfies both the standard conditions stated in the Introduction and the following additional conditions:

V. The dispersal kernel $\mathbf{K}(z, x)$ is determined by a number of spatially varying parameters $\alpha^j(x)$. These parameters, together with the elements $A^{i,j}(x)$ of the intrinsic population projection matrix $\mathbf{A}(x) = \mathbf{B}(\mathbf{0}, x)$, are small bounded perturbations from their spatial mean, i.e.

$$\alpha^i(x) = \alpha_0^i(1 + \epsilon q_1^i(x)) \text{ and } A^{j,k}(x) = A_0^{j,k}(1 + \epsilon Q_1^{j,k}(x)),$$

where $A_0^{j,k}$ and $\alpha_0^i$ are the spatial averages of the demographic and dispersal parameters. The relative heterogeneity coefficient $\epsilon$ satisfies $\epsilon \ll 1$ and the relative perturbations $q_1^j(x), Q_1^{i,j}(x)$ are O(1) and satisfy

$$\int_0^L q_1^i(x)\mathrm{d}x = 0 \ , \qquad \int_0^L Q_1^{j,k}(x)\mathrm{d}x = 0 \ ,$$

where $L$ is the period of the landscape. This allows the linearised population projection matrix to be written as

$$\mathbf{A}(x) = \mathbf{A}_0 + \epsilon \mathbf{A}_0 \circ \mathbf{Q}_1(x) \ .$$

and by taking its Taylor series (see Appendix A), we can write the dispersal kernel as

$$\mathbf{K}(z, y) = \mathbf{K}_0(z) + \epsilon \sum_{j=1}^{n} q_1^j(y)\mathbf{K}^j(z) + \frac{1}{2}\epsilon^2 \sum_{i,j=1}^{n} q_1^i(y)q_1^j(y)\mathbf{K}^{i,j}(z) + \mathrm{O}(\epsilon^3) \ .$$

For ease of notation, we use $\mathcal{F} = \left\{\alpha^i, A^{j,k}\right\}_{i,j,k=1,\cdots}$ to refer to these *landscape* parameters (in the context of the IDE model, the growth and dispersal parameters uniquely define the landscape).

VI. The spatially varying parameters $\alpha^j(x)$ and $A^{i,j}(x)$ are $L$-periodic for some $L \in (0, \infty)$, for example

$$\alpha^j(x + L) = \alpha^j(x) \quad \text{for all } x \in \mathbb{R} \ .$$

Conditions I, II and VI guarantee that we have solutions with a well-defined asymptotic wave-speed. Conditions III and IV guarantee that these will be equal to the asymptotic wave-speeds of solutions to the linearisation of (1) around $\mathbf{u}^t(x) = 0$ with initial compact support [30]. Condition V enables us to use regular perturbation methods. We will assume the additional conditions (V-VI) for IDEs on periodic landscapes, but will assume only a modified form of Condition V (that the homogeneous parameters are the spatial averages of the parameters over the whole landscape) when considering non-periodic landscapes.

The linearisation of (1) is

$$\mathbf{u}^{t+1}(x) = \int_{-\infty}^{\infty} \left[\mathbf{K}(x - y, y) \circ \mathbf{A}(y)\right] \mathbf{u}^t(y) \, \mathrm{d}y \ . \tag{4}$$

where $\mathbf{A}(x)$ is the linearisation of $\mathbf{B}(\mathbf{u}, x)$ around $\mathbf{u} = \mathbf{0}$.

For each linearised IDE (4) and each value of $\epsilon$ there is a family of periodic travelling-wave (PTW) solutions

$$\mathbf{u}(t,x) = \exp\left(s(c(s,\epsilon)t - x)\right)\boldsymbol{\phi}^s(x) \ , \tag{5}$$

where $s$ is the travelling wave's decay rate (its average steepness), $c(s,\epsilon)$ is the wave-speed and $\boldsymbol{\phi}^s(x)$ is a vector valued function on $[0,L)$. The asymptotic wave-speed is given by

$$\hat{c}(\epsilon) = \min_{s>0}\left[c(s,\epsilon)\right] \ . \tag{6}$$

Substituting (5) into the linearised IDE (4), we get a *dispersion relation*, which gives the wave-speed $c(s,\epsilon)$ in terms of an eigenvalue of a linear operator $F_s$. Since our landscapes have the form $\mathcal{F} = \mathcal{F}_0 + \epsilon\mathcal{F}_1$ where $\epsilon \ll 1$ and the spatial average of $\mathcal{F}_1$ is zero (Condition V), we can use regular perturbation theory to find the expansion for the wave-speeds (see Appendix B). We find that, for any IDE satisfying conditions I-VI, the wave-speed function $c(s,\epsilon)$ of the heterogeneous problem differs by only $\mathrm{O}(\epsilon^2)$ from the wave-speed function $c(s,0)$ of the spatially averaged homogeneous IDE with landscape $\mathcal{F}_0$, i.e.

$$c(s,\epsilon) = c(s,0) + \mathrm{O}(\epsilon^2) \quad \text{as} \quad \epsilon \to 0 \tag{7}$$

where $c(s,0)$ is the asymptotic wave-speed for the model with homogeneous parameters $\mathcal{F}_0$. By Condition II, we have that

$$\hat{c}(0) < \lim_{s\to\infty} c(s,0) \ .$$

This enables us to derive the stronger condition (see Appendix B) that

$$\hat{c}(\epsilon) = \hat{c}(0) + \mathrm{O}(\epsilon^2) \quad \text{as} \quad \epsilon \to 0 \ .$$

### *2.2. Wave-Speed Approximation for Stage-Structured Periodic Landscapes*

We have seen that the homogeneous approximation is better than expected (the error scales with the square of the relative heterogeneity coefficient $\epsilon^2$ rather than $\epsilon$). However, as $\epsilon$ is increased, the homogeneous approximation becomes less accurate. When this occurs, or a more exact result is required, we can find a second order approximation. To do this, we use the asymptotic analysis developed in the previous section and in Appendix B to find the coefficient of the $\mathrm{O}(\epsilon^2)$ term in the expansion of the wave-speed $\hat{c}(\epsilon)$ for non stage-structured and stage-structured populations. A full derivation of this approximation is given for Stage-Structured IDEs in Appendix C. We find that the $\mathrm{O}(\epsilon^2)$ approximation $\hat{c}_2(\epsilon)$ to the asymptotic wave-speed

is given by

$$\hat{c}_2(\epsilon) = \min_{s>0} \left\{ \frac{1}{s} \log \left( \tilde{\boldsymbol{\psi}}_s \cdot \left[ \mathbf{M}_0(s) \circ \mathbf{A}_0 + \epsilon^2 \mathbf{H}_2(s) \right] \boldsymbol{\psi}_s \right) \right\} \tag{8}$$

where $\mathbf{M}_0(s)$ is the moment generating function of the homogeneous kernel matrix $\mathbf{K}_0(z)$ and $\mathbf{A}_0$ is the homogeneous intrinsic population projection matrix. $\tilde{\boldsymbol{\psi}}_s$ and $\boldsymbol{\psi}_s$ are left and right eigenvectors of $\mathbf{M}_0(s) \circ \mathbf{A}_0$ chosen such that $\tilde{\boldsymbol{\psi}}_s \cdot \boldsymbol{\psi}_s = 1$, $\epsilon$ is the parameter determining the relative scale of the heterogeneity and $\mathbf{H}_2(s)$ is

$$\begin{aligned} \mathbf{H}_2(s) = \sum_{n \neq 0} \Bigg( & \left[ \mathbf{A}_0 \circ \left( \mathbf{M}_0(s) \circ \mathbf{C}_{-n} + \sum_{j=1}^{n} \gamma_{-n}^j \mathbf{M}^j(s) \right) \right] \left[ \mathbf{A}_0 \circ \left( \mathbf{M}_0(s) - \mathbf{M}_0 \left( s - \frac{2\pi i n}{L} \right) \right) \right]^{-1} \\ & \cdot \left[ \mathbf{A}_0 \circ \left( \mathbf{M}_0 \left( s - \frac{2\pi i n}{L} \right) \circ \mathbf{C}_n + \sum_{j=1}^{n} \gamma_n^j \mathbf{M}^j \left( s - \frac{2\pi i n}{L} \right) \right) \right] \\ & + \left[ \mathbf{A}_0 \circ \left( \sum_{j=1}^{n} \gamma_{-n}^j \mathbf{M}^j(s) \circ \mathbf{C}_n + \frac{1}{2} \sum_{i,j=1}^{n} \gamma_{-n}^i \gamma_n^j \mathbf{M}^{i,j}(s) \right) \right] \Bigg) \quad . \end{aligned} \tag{9}$$

$\mathbf{M}^j(s)$ is the moment generating function of the first derivative of the kernel $\mathbf{K}$ with respect to $q^j$, $\mathbf{M}^{i,j}(s)$ is the moment generating function of the second derivative of $\mathbf{K}$ with respect to $q^i$ and $q^j$, and $\mathbf{C}_n$ and $\gamma_n^j$ are the coefficients in the Fourier series of $\mathbf{Q}_1(x)$ and $q_1^j(x)$, i.e.

$$\mathbf{Q}_1(x) = \sum_{n \neq 0} \mathbf{C}_n \exp\left( \frac{2\pi i n x}{L} \right) \quad \text{and} \quad q_1^j(x) = \sum_{n \neq 0} \gamma_n^j \exp\left( \frac{2\pi i n x}{L} \right) \quad .$$

*2.3. Wave-Speed Approximation for Non-Stage-Structured Periodic Landscapes*

The second order approximation presented in the previous subsection is in general rather complicated, but in the absence of stage-structure, the approximation (8) simplifies to

$$\hat{c}_2(\epsilon) = \min_{s>0} \left\{ \frac{1}{s} \log \left( r_0 M_0(s) + \epsilon^2 H_2(s) \right) \right\} \quad , \tag{10}$$

where $r_0$ is the intrinsic population growth rate, $M_0(s)$ is the moment generating function of the homogeneous kernel $K_0(z)$ and $H(s)$ is given by

$$H_2(s) = r_0 \sum_{n\neq 0} \left( \frac{\left(C_{-n}M_0(s) + \sum_{j=1}^n \gamma_{-n}^j M^j(s)\right)\left(C_n M_0\left(s-\frac{2\pi i n}{L}\right) + \sum_{j=1}^n \gamma_n^j M^j\left(s-\frac{2\pi i n}{L}\right)\right)}{M_0(s) - M_0\left(s-\frac{2\pi i n}{L}\right)} + \sum_{j=1}^n \gamma_{-n}^j M^j(s) C_n + \frac{1}{2}\sum_{i,j=1}^n \gamma_{-n}^i \gamma_n^j M^{i,j}(s) \right) \quad , \tag{11}$$

where $M^j(s)$ is the moment generating function of the first derivative of the kernel $K$ with respect to $q^j$, $M^{i,j}(s)$ is the moment generating function of the second derivative of $K$ with respect to $q^i$ and $q^j$, and where the $C_n$ and $\gamma_n^j$ are the coefficients in the Fourier series of $Q_1(x)$ and $q_1^j(x)$, i.e.

$$Q_1(x) = \sum_{n\neq 0} C_n \exp\left(\frac{2\pi i n x}{L}\right) \quad \text{and} \quad q_1^j(x) = \sum_{n\neq 0} \gamma_n^j \exp\left(\frac{2\pi i n x}{L}\right) \quad .$$

*2.4. Extension to Non-Periodic Landscapes*

In the previous three subsections, we showed analytically that the homogeneous approximation is better than expected for periodic landscapes with small $\epsilon$ and derived a second order approximation to the wave-speed for periodic landscapes. To do this, we have required the landscape to be periodic. We now discuss the possibility of extending these results to non-periodic landscapes.

For periodic landscapes, we can assume that solutions to the linearised IDE are periodic travelling waves. This allows us to formulate a dispersion relation (the eigenvalue problem) for the wave-speed $c(s)$ of the solution to the linearised IDE for each value of the decay rate $s$. We can then take the minimum of $c(s)$ as the asymptotic wave-speed for solutions with initial conditions with compact support.

If the landscape is non-periodic (e.g. stochastically generated or quasi-periodic), then these methods cannot be applied. However, while it is not clear whether the approximation presented in §2.3 can be generalised to non-periodic landscapes, through the numerical simulations presented in §3.2 we see that the wave-speeds of solutions to IDEs on weakly heterogeneous stochastically-generated landscapes differ from their spatial homogenisations by $o(\epsilon)$ (i.e. as $\epsilon$ is made arbitrarily small, the difference becomes smaller than any factor than $\epsilon$). In §3.2 we will consider IDEs on landscapes satisfying conditions I-IV (the conditions in the Introduction, but not in §2.1) and an additional condition:

V.b. The dispersal kernel $\mathbf{K}(z,x)$ is determined by a number of spatially varying parameters $\alpha^j(x)$. These parameters, together with the elements $A^{i,j}(x)$ of the intrinsic population projection matrix $\mathbf{A}(x) = \mathbf{B}(\mathbf{0},x)$, are small bounded perturbations from their spatial mean, i.e.

$$\alpha^i(x) = \alpha_0^i(1+\epsilon q_1^i(x)) \text{ and } A^{j,k}(x) = A_0^{j,k}(1+\epsilon Q_1^{j,k}(x))$$

where the relative heterogeneity coefficient $\epsilon \ll 1$ and the relative perturbations $q_1^j(x), Q_1^{i,j}(x)$ are O(1) and satisfy

$$\int_{-\infty}^{\infty} q_1^i(x)\mathrm{d}x = 0 \ , \qquad \int_{-\infty}^{\infty} Q_1^{j,k}(x)\mathrm{d}x = 0 \ .$$

## 3. Examples

In this section, we consider two non-stage structured examples. In the first example (§3.1), we compare the simulated wave-speeds of solutions to IDEs on periodic landscapes with the homogeneous (zeroth order) and with the second order approximation introduced in §2.2. We show that both approximations are accurate for a range of $\epsilon$, with the second order approximation being more accurate, and appropriate for larger values of $\epsilon$. In the second example (§3.2), we show that the wave-speeds of IDE solutions on stochastically generated (non-periodic) landscapes also exhibit $\mathrm{o}(\epsilon)$ dependence on the relative heterogeneity coefficient $\epsilon$ and therefore that the homogeneous approximation is appropriate for at least some stochastically generated landscapes with very low environmental variation.

For the periodic example, we find the second order approximation presented in §2.3 for populations with Gaussian and Laplace kernels on an infinite landscape of two types of alternating regions of equal size, in which the growth/dispersal parameters take different sets of values. We compare this with the asymptotic wave-speeds of simulated solutions to (1), showing that this approximation is accurate. For the non-periodic example, we use numerical simulation to find the asymptotic wave-speeds of (1) with landscapes of two types of alternating region in which the size of each individual region is randomly generated from the Exponential distribution, to show that the asymptotic wave-speeds of IDEs on non-periodic landscapes exhibit $\mathrm{o}(\epsilon)$ sensitivity to the relative heterogeneity coefficient $\epsilon$.

In this paper, we have derived an approximation to the wave-speed on general (stage-structured populations), but in the interests of brevity, detail only non stage-structured examples. For these examples, we use the Beverton-Holt growth function for $\mathbf{B}(\mathbf{u}^t(x), x)$. This has been widely used in population modelling (e.g. for plants, see [31]), with the population after the growth phase being given by the current population $u$ multiplied by the growth rate

$$f(u) = \frac{r}{1+u} \ .$$

where $u$ is the scalar population before the growth phase and $r$ is the zero-population growth rate ($f(0) = r$). Since the approximation depends only on the zero-population growth rate, we could have used any growth function satisfying Condition II in §2.1 [17]. For both the periodic and non-periodic examples, we consider the same three landscape scenarios:

1. Only growth is varied and $(m_r, m_\alpha) = (1, 0)$ (Figure 1a,b)
2. Only dispersal is varied and $(m_r, m_\alpha) = (0, 1)$ (Figure 1c,d)
3. Growth and dispersal are varied and correlated and $(m_r, m_\alpha) = (1, 1)$ (Figure 1e,f)

where $m_r$ and $m_\alpha$ are indicators of the relative strength of the heterogeneity in the growth and dispersal parameters respectively.

### *3.1. Periodic Landscape*

We consider a non stage-structured population on a landscape of two alternating types of region of equal size. For each landscape considered, dispersal is given by either the Gaussian or Laplace kernel. The growth and dispersal parameters at location $x \in \mathbb{R}$ depend only on which type of region $x$ is in.

#### *3.1.1. Derivation of the Analytical Approximation*

We calculate the analytical approximation (8) for a landscape of two types of alternating region with either a Gaussian or Laplace dispersal kernel. The non-structured growth rate $r(x)$ is given by

$$r(x) = \begin{cases} r_0(1 + \epsilon m_r) & \text{for } x \in \left[nL, nL + \frac{L}{2}\right) \\ r_0(1 - \epsilon m_r) & \text{for } x \in \left[nL + \frac{L}{2}, (n+1)L\right) \end{cases},$$

where $r_0$ is the spatial mean of the growth rate and $L$ is the landscape period. The mean dispersal distance $\alpha(x)$ is given by

$$\alpha(x) = \begin{cases} \alpha_0(1 + \epsilon m_\alpha) & \text{for } x \in \left[nL, nL + \frac{L}{2}\right) \\ \alpha_0(1 - \epsilon m_\alpha) & \text{for } x \in \left[nL + \frac{L}{2}, (n+1)L\right) \end{cases},$$

where $\alpha_0$ is the spatial mean of $\alpha(x)$ and where $m_r$ and $m_\alpha$ are the strengths of the growth and dispersal heterogeneity. Therefore, using the definitions for the non-stage-structured approximation in §2.3, $Q_1(x)$ and $q_1(x)$ are given by

$$Q_1(x) = \begin{cases} m_r & \text{for } x \in \left[nL, nL + \frac{L}{2}\right) \\ -m_r & \text{for } x \in \left[nL + \frac{L}{2}, (n+1)L\right) \end{cases} \quad \text{and} \quad q_1(x) = \begin{cases} m_\alpha & \text{for } x \in \left[nL, nL + \frac{L}{2}\right) \\ -m_\alpha & \text{for } x \in \left[nL + \frac{L}{2}, (n+1)L\right) \end{cases}.$$

Expressing $Q_1(x)$ and $q_1(x)$ as Fourier series,

$$Q_1(x) = \sum_{n \in \text{Odd}} \frac{2m_r}{\pi i n} \exp\left(\frac{2\pi i n x}{L}\right) \quad \text{and} \quad q_1(x) = \sum_{n \in \text{Odd}} \frac{2m_\alpha}{\pi i n} \exp\left(\frac{2\pi i n x}{L}\right)$$

so

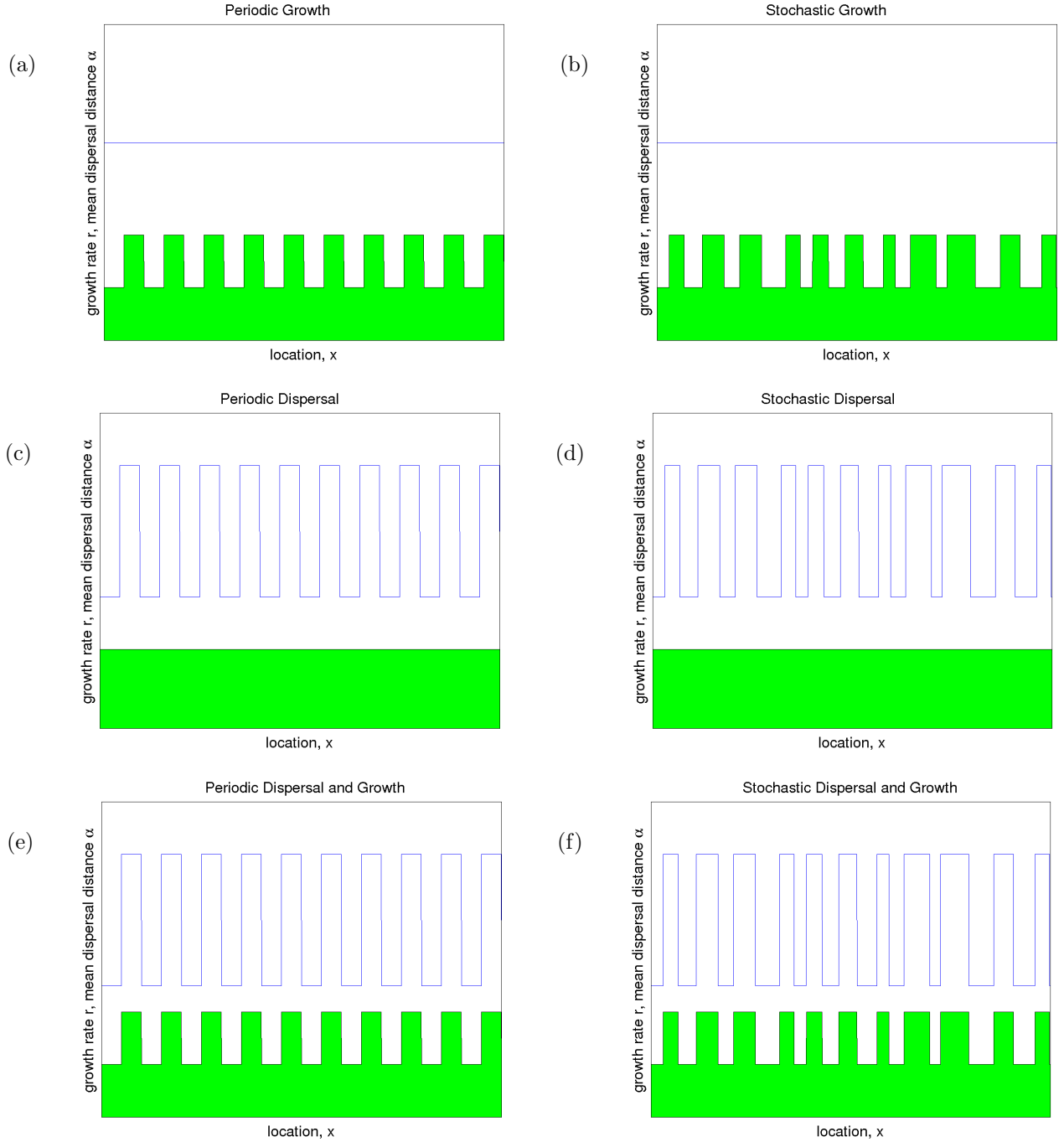


Figure 1: The intrinsic growth rate $r$ (solid area, green online) and the mean dispersal distance $\alpha$ (solid line, blue online) for the three landscape scenarios considered for the non-stage structured examples with periodic (a),(c),(e) and stochastic (b),(d),(f) landscapes. In (a),(b) only the intrinsic growth rate $r$ depends on the region type. In (c),(d) only the mean dispersal distance $\alpha$ depends on region type. In (e),(f) both parameters depend on region type. The landscapes shown here have $\epsilon = 0.333$. When growth and dispersal are both varied, as in (e),(f), they need not be correlated but we consider the correlated case as an example.

$$C_n = \begin{cases} \frac{2m_r}{n\pi i} & \text{if n is odd} \\ 0 & \text{if n is even} \end{cases} \quad \text{and} \quad \gamma_n = \begin{cases} \frac{2m_\alpha}{n\pi i} & \text{if n is odd} \\ 0 & \text{if n is even} \end{cases} .$$

Substituting this into (9), we get

$$\begin{aligned} H_2(s) =& r_0 \sum_{n\in\text{Odd}} \frac{4}{\pi^2 n^2} \left( \left[ m_r M_0(s) + m_\alpha M^1(s) \right] \left[ M_0(s) - M_0\left( s - \frac{2\pi i n}{L} \right) \right]^{-1} \right. \\ & \left. \cdot \left[ m_r M_0\left( s - \frac{2\pi i n}{L} \right) + m_\alpha M^1\left( s - \frac{2\pi i n}{L} \right) \right] + m_r m_\alpha M^1(s) + \frac{m_\alpha^2}{2} M^{1,1}(s) \right) . \end{aligned} \tag{12}$$

To compare this result with numerical simulations, we evaluate this for some specific kernels. We choose the widely used Gaussian and Lapalce kernels due to their analytical tractability. The Gaussian dispersal kernel is given in terms of the distance $z = x - y$ and the dispersal heterogeneity function $q(x) := 1 + q_1(x)$ (see Appendix A),

$$K(z, q) = \frac{1}{\alpha_0 q \sqrt{2\pi}} \exp\left( \frac{-z^2}{2(\alpha_0 q)^2} \right)$$

with the first $K^1(z, 1)$ and second $K^{1,1}(z, 1)$ derivatives of the Gaussian kernel $K(z, q)$ with respect to $q$ evaluated at $q = 1$

$$K^1(z, 1) = \frac{1}{\alpha_0 \sqrt{2\pi}} \left( \frac{z^2}{\alpha_0^2} - 1 \right) \exp\left( \frac{-z^2}{2\alpha_0^2} \right)$$

$$K^{1,1}(z, 1) = \frac{1}{\alpha_0 \sqrt{2\pi}} \left( \frac{z^4}{\alpha_0^4} - 5\frac{z^2}{\alpha_0^2} + 2 \right) \exp\left( \frac{-z^2}{2\alpha_0^2} \right) .$$

The Moment Generating Functions $M_0(s)$, $M^1(s)$ and $M^{1,1}(s)$ of $K_0(z) = K(z, 1)$, $K^1(z)$ and $K^{1,1}(z)$ are

$$M_0(s) = \exp\left( \frac{\alpha_0^2 s^2}{2} \right) \quad M^1(s) = \alpha_0^2 s^2 \exp\left( \frac{\alpha_0^2 s^2}{2} \right)$$

$$M^{1,1}(s) = \left( \alpha_0^2 s^2 + \alpha_0^4 s^4 \right) \exp\left( \frac{\alpha_0^2 s^2}{2} \right)$$

and $H_2(s)$ is given by

$$H_2(s) = r_0 \sum_{n\in \text{Odd}} \frac{4}{\pi^2 n^2} \left( \left[ m_r + m_\alpha \alpha_0^2 s^2 \right] \left[ \exp\left( \frac{2\pi i n \alpha_0^2 s}{L} + \frac{2\pi^2 n^2 \alpha_0^2}{L^2} \right) - 1 \right]^{-1} \right.$$
$$\left. \cdot \left[ m_r + m_\alpha \alpha_0^2 \left( s - \frac{2\pi i n}{L} \right)^2 \right] + m_r m_\alpha \alpha_0^2 s^2 + \frac{m_\alpha^2}{2} \left( \alpha_0^2 s^2 + \alpha_0^4 s^4 \right) \right) \exp\left( \frac{\alpha_0^2 s^2}{2} \right) \quad . \tag{13}$$

The second kernel we consider is the Laplace dispersal kernel, which is given by

$$K(z,q) = \frac{1}{2\alpha_0 q} \exp\left( \frac{-|z|}{\alpha_0 q} \right)$$

with the first $K^1(z,1)$ and second $K^{1,1}(z,1)$ derivatives of the Laplace kernel $K(z,q)$ with respect to $q$ evaluated at $q = 1$

$$K^1(z,1) = \frac{1}{2\alpha_0} \left( \frac{|z|}{\alpha_0} - 1 \right) \exp\left( \frac{-|z|}{\alpha_0} \right)$$

$$K^{1,1}(z,1) = \frac{1}{2\alpha_0} \left( \frac{|z|^2}{\alpha_0^2} - \frac{4|z|}{\alpha_0} + 2 \right) \exp\left( \frac{-|z|}{\alpha_0} \right) \quad .$$

The Moment Generating Functions $M_0(s)$, $M^1(s)$ and $M^{1,1}(s)$ of $K_0(z) = K(z,1)$, $K^1(z)$ and $K^{1,1}(z)$ are

$$M_0(s) = \frac{1}{1 - s^2\alpha_0^2} \quad M^1(s) = \frac{2s^2\alpha_0^2}{(1 - s^2\alpha_0^2)^2}$$

$$M^{1,1}(s) = \frac{2s^2\alpha_0^2}{(1 - s^2\alpha_0^2)^2} + \frac{8s^4\alpha_0^4}{(1 - s^2\alpha_0^2)^3}$$

and $H_2(s)$ is given by

$$H_2(s) = r_0 \sum_{n\in \text{Odd}} \frac{4}{\pi^2 n^2} \left( \frac{L^2}{4\pi\alpha_0^2 n\,(\pi n + iLs)} \left[ m_r + \frac{2m_\alpha s^2 \alpha_0^2}{(1 - s^2\alpha_0^2)} \right] \left[ m_r + \frac{2m_\alpha \left( s - \frac{2\pi i n}{L} \right) \alpha_0^2}{\left( 1 - \left( s - \frac{2\pi i n}{L} \right)^2 \alpha_0^2 \right)^2} \right] \right.$$
$$\left. + \frac{m_\alpha s^2 \alpha_0^2}{(1 - s^2\alpha_0^2)^2} \left[ 2m_r + m_\alpha \left( 1 + \frac{4s^2\alpha_0^2}{1 - s^2\alpha_0^2} \right) \right] \right) \quad . \tag{14}$$

*3.1.2. Numerical Results*

In this section, we present the numerical errors of the homogeneous and second order approximations for a range of parameters and scenarios. We simulate solutions to (1) for non stage-structured populations with Gaussian and Laplace dispersal kernels and Beverton-Holt growth function on an alternating landscape with two types of region of equal size. We measure the wave-speed $c^*$ of the simulation by finding the location of the wave-front (the largest value of $x$ where the population density is greater than some threshold value $\mu$)

for each $t$ and using linear regression to fit a constant wave-speed for the values of $t$ for which the wave-front has settled into a periodic travelling wave (see Appendix D). We calculate the relative error of the simulated wave-speed when compared to both the homogeneous approximation $\hat{c}_0$, and the second order analytical approximation $\hat{c}_2(\epsilon)$ presented in (10). We take the spatial mean $\alpha_0$ of the dispersal parameter to be fixed at $\alpha_0 = 1$ and the mean growth rate to be fixed at $r_0 = 1.2$ and vary the relative heterogeneity coefficient $\epsilon$ and the landscape period $L$. In §3.3, we fix $\epsilon = 0.3$ and vary $r$ and $L$ for Gaussian landscapes and compare the effect of heterogeneity (compared to homogeneous landscapes) for the periodic and non-periodic landscapes. In both this section and the following one, we will explore each of the three periodic landscape scenarios presented in Figure 1.

The relative error $E_j$ of the $j$-th order approximation (for $j = 0, 2$) is given in terms of the approximation $\hat{c}_j$ and the simulated wave-speed $c^*$ by

$$E_j = \frac{\hat{c}_j - c^*}{c^*} \ .$$

$E_j$ is a measure of the accuracy of the approximation, and is positive when the approximation is an over-estimate of the numerical wave-speed, and negative when it is an under-estimate. Where $E_j$ is small, $\hat{c}_j$ is a good approximation to the simulated wave-speed $c^*$ and hence the asymptotic wave-speed of solutions to (1).

In Figures 2 and 3, we present the relative error of the homogeneous and second order approximations to the wave-speed for a range of values of landscape period $L$ and relative heterogeneity coefficient $\epsilon$ and consider values in the domain $0 < L \leq 10, 0 < \epsilon < 0.5$. We consider Gaussian (Figure 2a,c,e and Figure 3a,c,e) and Laplace (Figure 2b,d,f and Figure 3b,d,f) dispersal kernels, and allow spatial heterogeneity only in the growth rate (Figure 2a,b and Figure 3a,b), only in the dispersal parameters (Figure 2c,d and Figure 3c,d) and in both growth and dispersal jointly (Figure 2e,f and Figure 3e,f).

In Figure 2, we see that, for all scenarios, the relative error $E_0 \sim \mathrm{o}(\epsilon)$ as $\epsilon \to 0$ (the difference can be made arbitrarily smaller than $\epsilon$ for sufficiently small $\epsilon$), that the relationship between $\epsilon$ and the wave-speed is monotone (except for a small region of parameter space in the top right of Figure 2e), and that the behaviour of $c^*$ as $\epsilon$ increases depends on the landscape period $L$. For the Laplace kernel the simulated wave-speeds for $\epsilon = 0$ are about 2% higher than the homogeneous approximation due to numerical error, which explains the small band of light blue for $\epsilon \sim 0$. We find that for $\epsilon < 0.3$, the absolute value of the relative error of the homogeneous approximation is less than 0.14. In §3.2, we will fix $\epsilon = 0.3$ and vary the mean growth rate $r$ and landscape period $L$ for the Gaussian kernel and the three landscape scenarios, to compare the behaviour in the periodic and stochastically generated landscape. Here (see Figure 5), we find that for $\epsilon = 0.3$, the relative change of the simulated wave-speed in the heterogeneous landscape when compared to the simulated

wave-speed in the homogeneous landscape is less than 0.21 for $r > 1.05$ in the range of parameters considered.

The homogeneous approximation is independent of $\epsilon$ and $L$, so is constant for the parameter values considered in Figure 2. Therefore, for these parameter values, the relationship between the relative error of the homogeneous approximation and the simulated wave-speed is linear. This allows us to use Figure 2 to consider the effects of $r$ and $L$ on the simulated wave-speed for the different kernels and heterogeneity scenarios. When only the growth rate varies spatially (Figures 2a,b), increased $\epsilon$ only affects the wave-speed for sufficiently large $L$, causing it to increase with $\epsilon$. On the other hand, when only the dispersal parameter varies spatially (Figures 2c,d), increased $\epsilon$ causes an increase only for samll $L$ and for large $L$, either has no effect (Laplace kernel, Figure 2d) or causes a decrease in wave-speed (Gaussian kernel, Figure 2c). When both growth and dispersal vary together, the effect of $\epsilon$ for each $L$ depends heavily on the type of kernel. For the Gaussian kernel, the wave-speed increases as $\epsilon$ increases for small $L$ and decreases for large $L$. For the Laplace kernel, the wave-speed increases with $\epsilon$ for all values of $L$ in the range considered.

In Figure 3, we plot the relative error $E_2$ of the second order approximation $\hat{c}_2(\epsilon)$. In Figures 3a,b only the intrinsic growth rate depends on the type of region (Figure 1a), in Figures 3c,d only the mean dispersal distance depends on the region type (Figure 1c), and in Figures 3e,f both the intrinsic growth rate $r$ and the mean dispersal distance $\alpha$ depend on region type, with one region type having higher $r$ and higher $\alpha$ than the other (Figure 1e). The populations corresponding to Figures 3a,c,d have Gaussian dispersal kernels and those considered in Figures 3b,d,e have Laplace dispersal kernels.

The relationship between the landscape period $L$, the relative heterogeneity coefficient $\epsilon$ and the accuracy of the second order approximation depends on which landscape scenario is being explored. When only growth or dispersal varies with the environment, the relative error is small for all values of $L$ and $\epsilon$ considered. When growth and dispersal are both varied, the relative error is small for $\epsilon < 0.3$ or small $L$, but becomes large when $\epsilon$ and $L$ are both large. This is due to the growth of higher order terms in the asymptotic expansion of the eigenvalue $\rho(s) = \mathrm{e}^{sc(s)}$ of the dispersion relation (B.1) in (C.5) with respect to $\epsilon$.

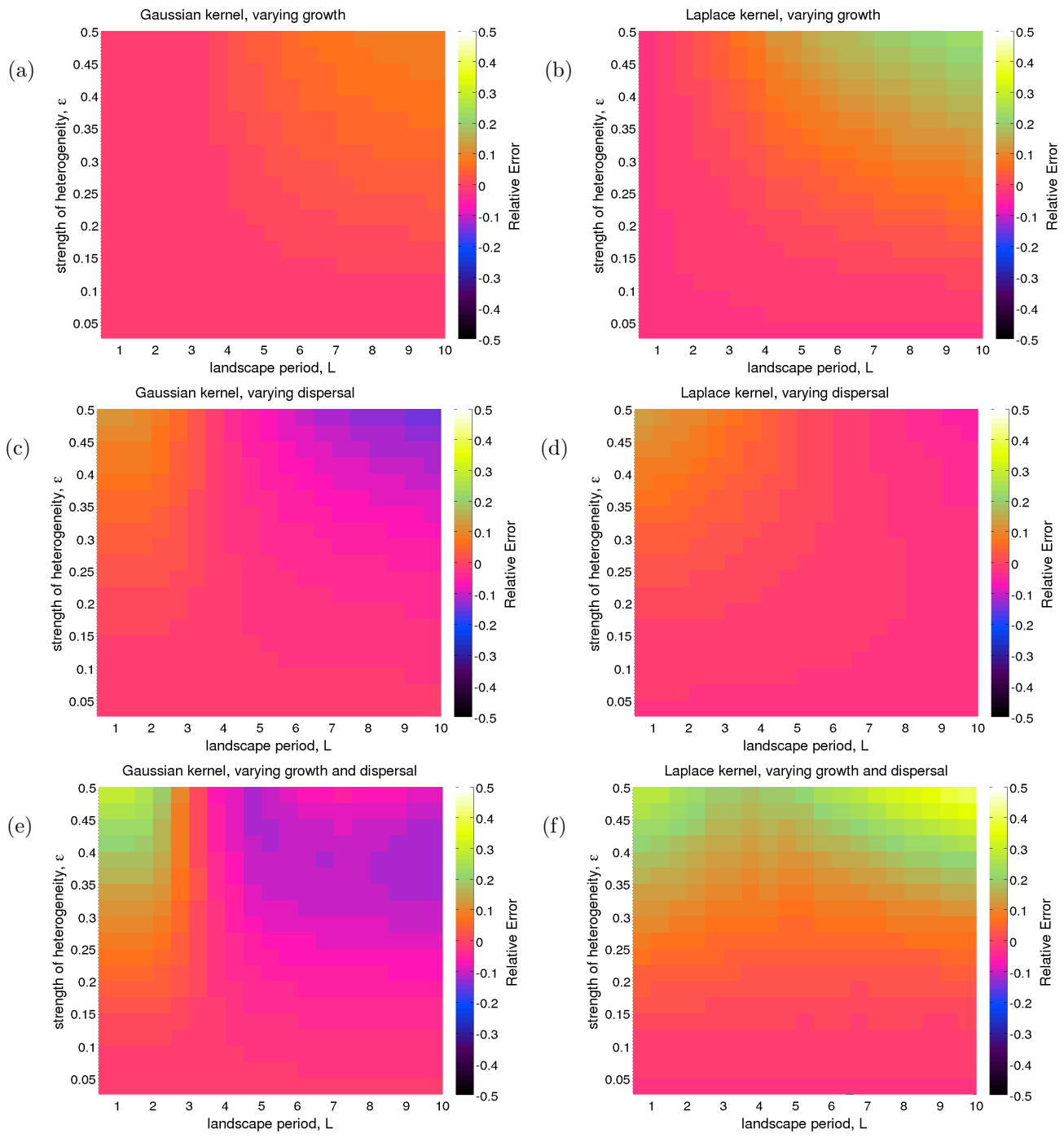


Figure 2: Relative Error of the homogeneous (zeroth order) approximation for Gaussian (a),(c),(e) and Laplace (b),(d),(f) kernels for a range of heterogeneity strength $\epsilon$ and landscape period $L$, where spatial heterogeneity is present in the growth rate (a),(b), the mean dispersal distance (c),(d) and both the growth rate and mean dispersal distance (e)-(f). The spatially averaged growth rate and the spatial average of the mean dispersal distances are $r_0 = 1.2$ and $\alpha_0 = 1$.

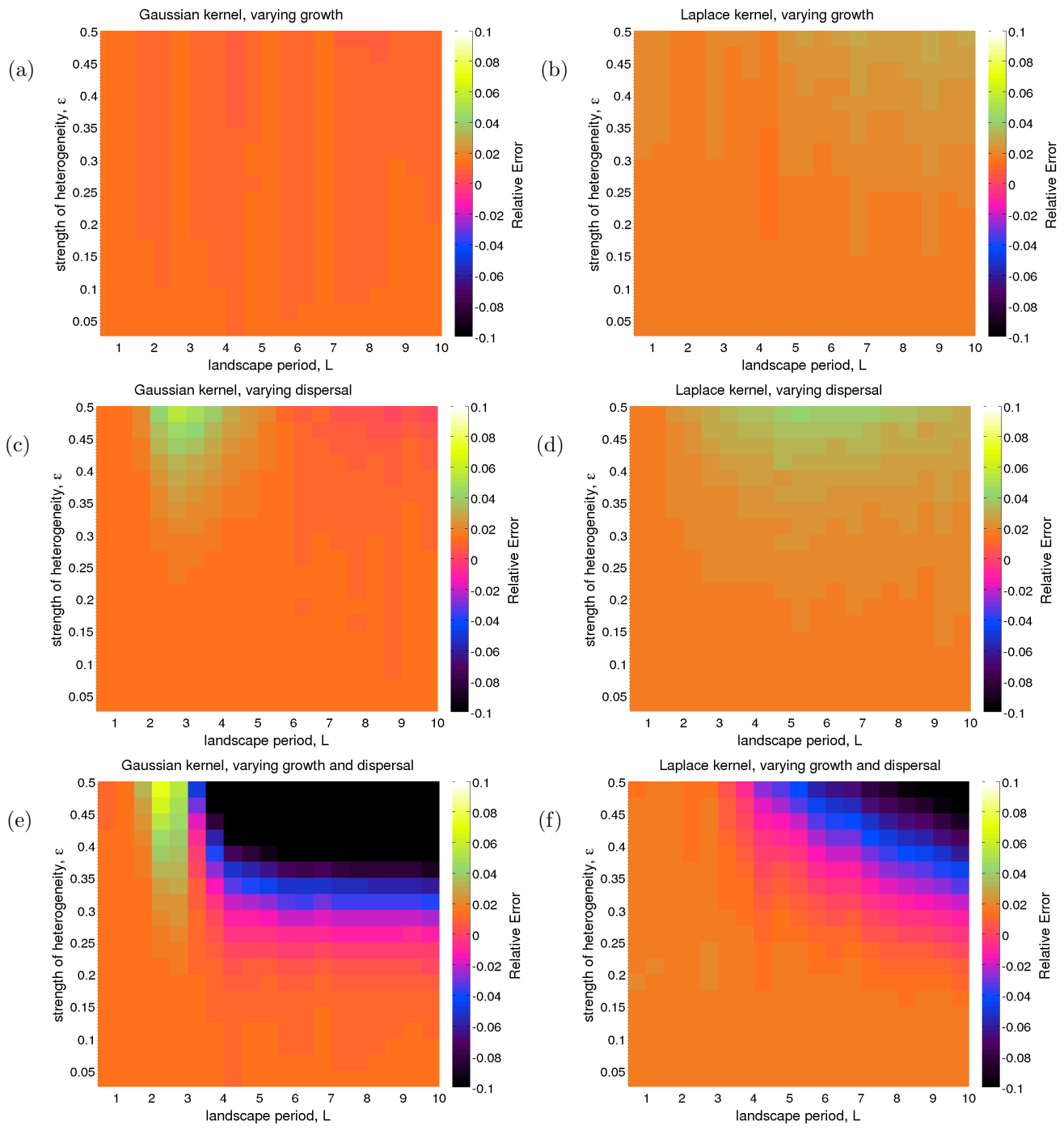


Figure 3: Relative Errors ($\min\{0.1, \max\{-0.1, E\}\}$) of the second order wave-speed approximation for Gaussian (a),(c),(e) and Laplace (b),(d),(f) kernels for a range of heterogeneity strength $\epsilon$ and landscape period $L$, where spatial heterogeneity is present in the growth rate (a),(b), the mean dispersal distance (c),(d) and both the growth rate and mean dispersal distance (e)-(f). The spatially averaged growth rate and the spatial average of the mean dispersal distances are $r_0 = 1.2$ and $\alpha_0 = 1$.

*3.2. Stochastic Landscape*

We now consider the relationship between the environmental variation coefficient $\epsilon$ and the spread rate in stochastically generated landscapes by numerically simulating solutions to IDEs on stochastic analogues of the periodic landscapes considered in §3.1 (where the landscapes consisted of two alternating types of region of equal size $L/2$). In the stochastically generated landscapes, the size of region (regardless of its type) is an independent random variable with mean $L/2$. We fix the distribution of the random variables as the uniform distribution on $[L/4, 3L/4]$. An advantage of the uniform distribution is that the lengths of the patches are bounded above by $3L/4$. This prevents populations becoming arbitrarily small in a region with low growth rate and the resulting difficulties in simulation. We take the representative value $r_0 = 1.5$ for the mean growth rate. More formally, the length of each region $L_j$ (irrespective of region type) is independently

$$L_j \sim \mathcal{U}\left(\frac{L}{4}, \frac{3L}{4}\right) \quad .$$

To explore the relationship between the environmental variation coefficient $\epsilon$ and the asymptotic wave-speed, we generated 50 landscapes with independently uniformly distributed region sizes for each combination of dispersal kernel, landscape scenario (spatially varying growth, spatially varying dispersal and both spatially varying growth and dispersal) and representative average landscape periods $L = 2$ and $L = 4$. We found that generating 50 landscapes for each scenario was sufficient in this case, as further runs did not change our conclusions. We simulated the IDE on each landscape for $0 \leq \epsilon \leq 0.5$. For each combination of kernel, landscape scenario and mean landscape period $L$ and each value of $\epsilon$, we take the average wave-speed for the different landscapes. We present these results in Figure 4 and find that for each kernel, heterogeneity scenario and landscape period, the change in mean wave-speed for values of $\epsilon$ close to zero is very small. For the parameters considered here, the relationship between $\epsilon$ and the wave-speed $c$ is found to be monotone increasing or decreasing and smooth.

We observe that the relationship between $\epsilon$ and the mean invasion speed is either convex with a minimum at $\epsilon = 0$ or concave with a maximum at $\epsilon = 0$. This shows that wave-speed sensitivity reduces massively for small $\epsilon$, demonstrating a dependence of the form $o(\epsilon)$ and thus a lack of sensitivity to sufficiently small perturbations of the landscape.

In Figure 5, we plot the relative change in wave-speed between the homogeneous landscape ($\epsilon = 0$) and a heterogeneous one ($\epsilon = 0.3$) for the periodic landscapes introduced in §3.1 and the stochastically generated landscapes introduced earlier in this section. We compare the homogeneous and heterogeneous wave-speeds for all three landscape scenarios in Figure 1 and for a range of values of mean growth rate and (mean) landscape period. We calculate the wave-speed for the stochastic case by taking the average wave-speed from simulations on fifty different landscapes. We present only the results for the Gaussian dispersal kernel, but

find a similar relationship between the periodic and stochastically generated plots for the Laplace kernel.

Where only the growth is varied (Figure 5a,b), the relative change in wave-speed is small for large growth rate $r_0 > 8$ or small landscape period ($L < 5$ for the periodic landscape, $L < 2$ for the stochastic landscape). The relative change is highest for the smallest values of $r_0$ and the largest values of $L$ studied ($r_0 \sim 1.5$ and $L \sim 20$). When heterogeneity is only in dispersal (Figure 5c,d), for both the periodic and stochastic example, increasing $L$ decreases, and increasing $r$ increases the relative change in wave-speed. For small values of $L$, invasions in the heterogeneous landscape are faster in than in the corresponding homogeneous one, but for larger values of $L$, heterogeneity slows invasions down. For intermediate $L$ ($L \sim 10$ for the periodic landscape and $L \sim 5$ for the stochastically generated landscape), there is no change in wave-speed between $\epsilon = 0$ and $\epsilon = 0.3$. When heterogeneity is present in both dispersal and growth (Figure 5e,f), the relationship between $r, L$ and the relative change in wave-speed between the homogeneous and heterogeneous landscape is more complex. For small $L$, the relative change is positive, and as $L$ increases the relative change becomes negative (as in the heterogeneous dispersal case). However, there is an additional positive peak for low $r_0$ and high $L$ (the same location as the peak for the heterogeneous growth case). This more complex behaviour is likely to be due to the combined effect of dispersal heterogeneity and growth heterogeneity.

When comparing the plots for periodic landscape (Figures 5a,c,e) and the corresponding plots for the stochastically generated landscapes (Figures 5b,d,f), the qualitative relationships between $r$, $L$ and the relative change in wave-speed are the same, but are quantitatively different. This suggests that the wave-speeds on stochastically generated landscapes have similar behaviour to wave-speeds on periodic landscapes, giving us greater confidence in extending our main result (that the difference between heterogeneous and homogeneous landscapes is $o(\epsilon)$) to non-periodic landscapes.

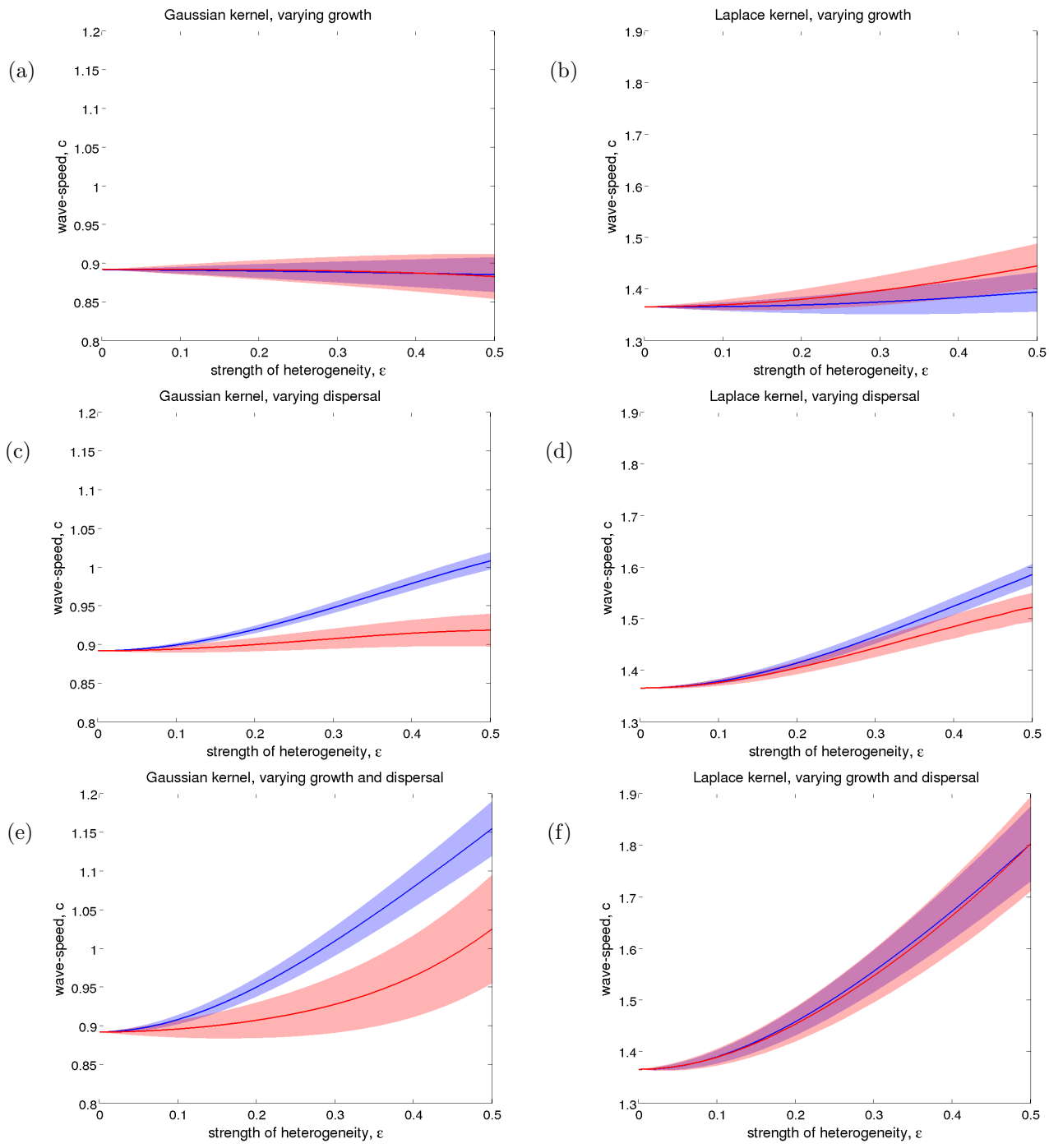


Figure 4: Mean (solid lines) simulated wave-speeds, with standard deviations (transparent) of IDEs for Gaussian (a),(c),(e) and Laplace (b),(d),(f) kernels with the spatial average of the mean dispersal distance $\alpha_0 = 1$ for landscape period $L = 2$ (blue) and $L = 4$ (red) on stochastically generated landscapes, where spatial heterogeneity is present in the growth rate (a),(b), the mean dispersal distance (c),(d) and both the growth rate and mean dispersal distance (e)-(f).

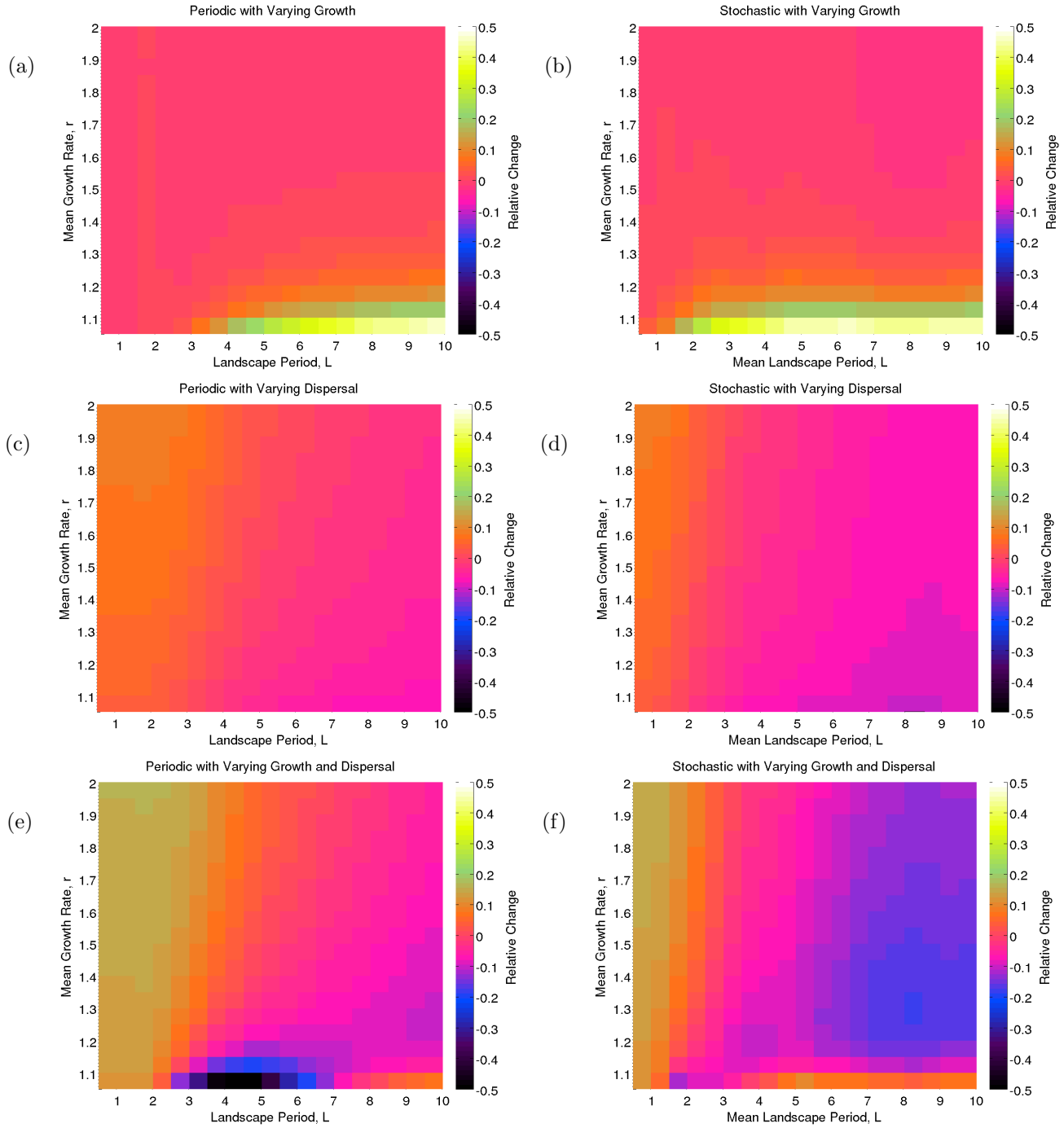


Figure 5: Relative change in the wave-speed of solutions to IDEs with $\epsilon = 0.3$ compared to the wave-speed of the corresponding homogeneous IDE (i.e. the same IDE with $\epsilon = 0$). The wave-speeds are for periodic (a),(c),(e) and the mean wave-speed of fifty stochastically generated (b),(d),(f) landscapes with Gaussian dispersal, where heterogeneity is present only in the growth (a),(b), where heterogeneity is present only in the dispersal (c),(d) and where heterogeneity is present both in the growth and dispersal (e),(f).

## 4. Discussion

In this paper, we have shown analytically that the wave-speeds of solutions to periodic IDEs with low environmental variation differ from the wave-speeds of solutions to their homogenisations by a factor proportional to $\epsilon^2$, where $\epsilon$ is the relative heterogeneity coefficient, and have shown numerically that a similar result (that the wave-speeds differ by a factor less than $\epsilon$) extends to the non-periodic landscapes considered. Through numerical simulations, we have found that for the Laplace and Gaussian dispersal kernels, with mean growth rate $r = 1.2$, spatial average of the mean dispersal distance $\alpha_0 = 1$ and relative heterogeneity coefficient $\epsilon < 0.3$ and a range of values of the landscape period $L$, the relative error of the homogeneous approximation is less than 15% (see Figure 2). Additionally, for the Gaussian kernel with $\alpha_0 = 1$, $\epsilon = 0.3$ and a range of values of $r_0$ and $L$ (with $r > 1.05$), the relative error is less than 21%. This means that the wave-speed of the invasion in homogeneous landscapes is often a very good approximation to the wave-speed even when $\epsilon$ is only moderately small. Additionally, our finding that the error was very small for $\epsilon \sim 0$ is in agreement with the analytical result.

This means that for small values of $\epsilon$, the homogeneous approximation is better than might initially be expected. Therefore, for any landscape with low environmental variation, with dispersal given by any exponentially bounded kernel, homogenising and using the comparatively simple formula for the asymptotic wave-speed $\hat{c}(0)$ in homogeneous landscapes may be a sensible approach to approximating the wave-speed $\hat{c}$. This is useful for ecologists studying real landscapes, as small variations can be averaged out, making the analytical calculations of the wave-speed much simpler. The straightforward homogeneous IDE can be implemented, as in previous ecological studies (e.g. [8, 10, 18]), by taking these average values to parametrise the IDE.

For more complex landscapes with large variation on small spatial scales but with less variation over large scales, it may be possible to combine the methods presented in this paper with the methods presented by Dewhirst and Lutscher [13] to justify the use of the homogeneous approximation. Dewhirst and Lutscher used Riemann sums to show that rapidly varying landscapes could be approximated by their homogenisation, but it seems reasonable that this could be extended to justify the removal of the rapidly oscillating frequencies from the Fourier decomposition of the landscape even in the presence of frequencies with larger periods. Assuming that the resulting smoothed landscape has low environmental variation, the analysis presented in this paper could be used to justify the homogeneous approximation and thus enable the comparatively simple expressions for the wave-speed derived by Kot [32] for non-stage-structured IDEs and by Neubert and Caswell [18] for stage-structured IDEs to be used to approximate the speeds of real spreading populations on complex heterogeneous landscapes.

For IDEs on periodic landscapes where more analytical accuracy is required, or the specific effects of the heterogeneity on the wave-speed are being studied, we have derived a second order approximation $\hat{c}_2(\epsilon)$ which

incorporates the $O(\epsilon^2)$ term in the asymptotic expansion of $\rho(s) = e^{sc(s)}$. We have found $\hat{c}_2(\epsilon)$ by linearising the IDE, considering periodic travelling wave solutions and using regular perturbation theory. Unlike the homogeneous approximation, the second order approximation has an $\epsilon$ dependence, so takes into account the details of the heterogeneity, but is much more complex than the homogeneous approximation. Numerically, we have found that for the Gaussian and Laplace kernels and $\epsilon < 0.3$, the relative error was less than 4% for $r_0 = 1.2$, $\alpha_0 = 1$ and a range of values of $L$, thus demonstrating a greater degree of accuracy.

While intrinsic stochasticity and variation have been found to reduce populations' spreading speeds [10, 33, 34], we have found that the effects of extrinsic/landscape variation to be more complex. Although the relationship between the heterogeneity coefficient $\epsilon$ and the wave-speed is monotone (Figures 2 and 4), the precise effect that increasing environmental variation has on the wave-speed has a complex dependence on the dispersal kernel and mean dispersal distance $\alpha_0$, the mean growth rate $r_0$ and the landscape period $L$. It is likely that this is due to a complex interplay between increasing isolation of suitable habitat as $\epsilon$ increases (which we would expect to reduce the spreading speed) and the clustering of good habitat (which we would expect to increase the spreading speed). Which of these effects is stronger depends on the values of $r_0$ and $L$ [35]. Therefore, to characterise the precise effects of increased $\epsilon$ on the spread rate accurately, it is necessary to characterise the precise shape of the dispersal kernel and the structure of the landscape (i.e. the way the growth and dispersal parameters vary spatially).

For both dispersal kernels in the periodic example, we have found (Figure 2) that for fixed mean growth rate $r_0 = 1.2$ that the effect of increased heterogeneity ($\epsilon$) depends on the landscape period $L$, the choice of dispersal kernel and the heterogeneity scenario (whether heterogeneity is present only in the growth rate, the dispersal parameters, or in both simultaneously). Additionally, we have found that for the Gaussian kernel and both periodic and stochastically generated landscapes (see Figure 5), that when $\epsilon$ is fixed and $r_0$ and $L$ vary, the relative change in wave-speed is qualitatively similar for the periodic and non-periodic cases. Additionally, in the case where growth and dispersal are heterogeneous and correlated, the relative change in wave-speed (as a function of $r_0$ and $L$) is the superposition (sum) of the relative changes in wave-speed for the cases where only growth or dispersal are heterogeneous. We hypothesise that this is due to the different relative strengths of the effects of spatially varying growth and dispersal for the two dispersal kernels. Therefore, accurately characterising the dispersal kernel, the degree and type of environmental variation and the dispersal pattern is of utmost importance when predicting the spread rate of a population.

In this paper, we have shown the $O(\epsilon^2)$ dependence of the wave-speed on the environmental variation coefficient for general stage-structured IDEs, but in the interests of brevity, have only considered non-stage-structured examples. We anticipate that the approximation would show similar effectiveness on stage-structured examples. Conversely, we have been able to show a lack of sensitivity in the wave-speed in non-periodic landscapes to $\epsilon$ numerically, but have not been able to do so analytically. In §3, due to their

wide use and analytical tractability, we have used the Laplace and Gaussian kernels. However, all the results presented here are valid for any of the more complex exponentially bounded kernels which are often used in ecology [36].

In summary, we have shown for periodic and non-periodic landscapes that the asymptotic wave-speed of the model shows a lack of sensitivity to the environmental variation coefficient $\epsilon$ and therefore that the simpler homogeneous approximation to the wave-speed is valid for landscapes with low environmental variation. For situations where more accuracy is required, we have derived a second order approximation to the wave-speed in terms of $\epsilon$ for periodic landscapes, and have shown it to be accurate through numerical simulation.

**Acknowledgements**

MAG acknowledges the support of a Natural Environment Research Council Doctoral Training Grant [grant number NE/J500045/1].

## Appendix A. Expansion of the Dispersal Kernel

The form of the stage-structured dispersal kernel $\mathbf{K}(x-y,y)$ of dispersers from point $y$ is dependent on the value of each of the scalar parameters $\alpha^1(y),\cdots,\alpha^n(y)$. Each of these take the form

$$\alpha^j(y) = \alpha_0^j[1+\epsilon q_1^j(y)]$$

where $q^j(y) \sim \mathrm{O}(1)$. At each $y$, the kernel can be written as

$$\begin{aligned}\mathbf{K}(z,y) &= \mathbf{K}(z,\alpha^1(y),\cdots,\alpha^n(y))\\ &= \mathbf{K}(z,\alpha_0^1 q^1,\cdots,\alpha_0^n q^n)\\ &= \mathbf{K}(z,\alpha_0^1[1+\epsilon q_1^1(y)],\cdots,\alpha_0^n[1+\epsilon q_1^n(y)])\ .\end{aligned}$$

We can expand the kernel in terms of its Taylor series in the variables $q^1,\cdots,q^n$,

$$\begin{aligned}\mathbf{K}(z,y) &= \mathbf{K}(z,\alpha_0^1,\cdots,\alpha_0^n) + \epsilon\sum_{j=1}^n q_1^j(y)\frac{\partial \mathbf{K}}{\partial q^j}(z,\alpha_0^1,\cdots,\alpha_0^n)\\ &\quad + \frac{1}{2}\epsilon^2\sum_{i,j=1}^n q_1^i(y)q_1^j(y)\frac{\partial^2\mathbf{K}}{\partial q^i\partial q^j}(z,\alpha_0^1,\cdots,\alpha_0^n) + \mathrm{O}(\epsilon^3)\\ &= \mathbf{K}_0(z) + \epsilon\sum_{j=1}^n q_1^j(y)\mathbf{K}^j(z) + \frac{1}{2}\epsilon^2\sum_{i,j=1}^n q_1^i(y)q_1^j(y)\mathbf{K}^{i,j}(z) + \mathrm{O}(\epsilon^3)\\ &= \mathbf{K}_0(z) + \epsilon\mathbf{K}_1(z,y) + \epsilon^2\mathbf{K}_2(z,y) + \mathrm{O}(\epsilon^3)\ .\end{aligned}$$

Since we are given that $\int_0^L q_1^j(y)\mathrm{d}y = 0$ (Condition V), the spatial average of $\mathbf{K}_1(z,x)$ in $x$ over $[0,L)$ is given by

$$\begin{aligned}\int_0^L \mathbf{K}_1(z,y)\mathrm{d}y &= \sum_{j=1}^{n}\left(\int_0^L q_1^j(y)\mathrm{d}y\right)\mathbf{K}^j(z)\\ &= 0\end{aligned}$$

for all $z \in \mathbb{R}$.

## Appendix B. Asymptotic Expansion of the Wave-speed

We substitute the periodic travelling wave solution

$$u(t,x) = \exp\left[s(c(s,\epsilon)t - x)\right]\boldsymbol{\phi}_s(x)$$

into the $L$-periodic linear IDE (4) to give us the dispersion relation

$$\exp\left[sc(s,\epsilon)\right]\boldsymbol{\phi}_s(x) = \int_{-\infty}^{\infty}\left[\mathbf{K}(x-y,y)\mathrm{e}^{s(x-y)} \circ \mathbf{A}(y)\right]\boldsymbol{\phi}_s(y)\,\mathrm{d}y \ . \tag{B.1}$$

on $x \in [0,L]$, with boundary conditions $\boldsymbol{\phi}_s(0) = \boldsymbol{\phi}_s(L)$. There is one additional degree of freedom in our choice of $\boldsymbol{\phi}_s(x)$, but this will be removed when we fix the size of the first term in its asymptotic expansion to be equal to 1. This dispersion relation has the general form

$$\rho(s,\epsilon)\boldsymbol{\phi}_s(x) = (F^\epsilon\boldsymbol{\phi}_s)(x) \ , \tag{B.2}$$

where the operator is an $\mathrm{O}(\epsilon)$ perturbation from the homogeneous spatial average over $[0,L]$. Hence we can write

$$F^\epsilon = F_0^\epsilon + \epsilon F_1^\epsilon + \mathrm{O}(\epsilon^2)$$

where the $\mathrm{O}(1)$ term corresponds to the unperturbed homogeneous case, i.e. $F_0^\epsilon = F^0$,

$$(F^0\mathbf{u})(x) = \int_{-\infty}^{\infty}\left[\mathbf{K}_0(x-y)\mathrm{e}^{s(x-y)} \circ \mathbf{A}_0\right]\mathbf{u}(y)\,\mathrm{d}y$$

where $\mathbf{A}_0$ is the spatial average of the intrinsic population projection matrix $\mathbf{A}(x)$ and $\mathbf{K}_0(z)$ is the spatially homogeneous dispersal kernel defined in Appendix A. We can therefore write

$$F^\epsilon = F^0 + \epsilon F_1^\epsilon + \mathrm{O}(\epsilon^2)$$

This is a regular perturbation problem, and can be solved by substituting asymptotic expansions of $\boldsymbol{\phi}_s(x)$ and $\rho(s,\epsilon)$ in $\epsilon$,

$$\begin{aligned}\boldsymbol{\phi}_s(x) =& \boldsymbol{\phi}_{s,0}(x) + \epsilon\boldsymbol{\phi}_{s,1}(x) + \epsilon^2\boldsymbol{\phi}_{s,2}(x) + \cdots \\ \rho(s,\epsilon) =& \rho_0(s) + \epsilon\rho_1(s) + \epsilon^2\rho_2(s) + \cdots \ .\end{aligned}$$

Substituting these into (B.2), the O(1) terms satisfy

$$\rho_0(s)\boldsymbol{\phi}_{s,0}(x) = (F^0\boldsymbol{\phi}_{s,0})(x) \ ,$$

i.e. $\rho_0(s)$ is the eigenvalue of the unperturbed homogeneous operator $F^0$,

$$\rho_0(s) = \rho(s,0)$$

and $\boldsymbol{\phi}_{s,0}$ is constant and equal to $\boldsymbol{\psi}_s$. In the inner product space $L^2([0,L))$, the adjoint operator $F^{0*}$ of $F^0$ is given by

$$(F^{0*}\mathbf{u})(x) = \int_{-\infty}^{\infty} \left[\mathbf{K}_0(x-y)\mathrm{e}^{s(x-y)} \circ \mathbf{A}_0\right]^T \mathbf{u}(y)\,\mathrm{d}y \ . \tag{B.3}$$

This operator has a constant eigenvector $\boldsymbol{\phi}^*_{s,0}$ corresponding to the principal eigenvalue $\rho(s,0)$. The O($\epsilon$) terms in the eigenvalue equation satisfy

$$(F^0 - \rho(s,0))\boldsymbol{\phi}_{s,1} + (F_1^\epsilon - \rho_1(s))\boldsymbol{\phi}_{s,0} = 0 \ .$$

Taking the inner product of this with $\boldsymbol{\phi}^*_{s,0}$, we find that

$$\langle\boldsymbol{\phi}^*_{s,0}|(F^0 - \rho(s,0))\boldsymbol{\phi}_{s,1}\rangle = \langle(F^{0*} - \rho(s,0))\boldsymbol{\phi}^*_{s,0}|\boldsymbol{\phi}_{s,1}\rangle = 0$$

and that

$$\langle\boldsymbol{\phi}^*_{s,0}|(F_1^\epsilon - \rho_1(s))\boldsymbol{\phi}_{s,0}\rangle = 0 \ ;$$

rearranging, this gives us an expression for $\rho_1(s)$,

$$\rho_1(s) = \frac{\langle\boldsymbol{\phi}^*_{s,0}|F_1^\epsilon\boldsymbol{\phi}_{s,0}\rangle}{\langle\boldsymbol{\phi}^*_{s,0}|\boldsymbol{\phi}_{s,0}\rangle} \ . \tag{B.4}$$

We find $\boldsymbol{\phi}^*_{s,0}$ and $\boldsymbol{\phi}_{s,0}$ to be constant and equal to $\tilde{\boldsymbol{\psi}}_s$ and $\boldsymbol{\psi}_s$ respectively. Without loss of generality, we

choose $\tilde{\boldsymbol{\psi}}_s \cdot \boldsymbol{\psi}_s = 1$, so

$$\rho_1(s) = \frac{1}{L}\int_0^L \tilde{\boldsymbol{\psi}}_s \cdot (F_1^\epsilon \boldsymbol{\psi}_s)(x)\mathrm{d}x \ . \tag{B.5}$$

To evaluate this, we need the expression for $(F_1^\epsilon \boldsymbol{\phi})(x)$, this is given by

$$\int_{-\infty}^{\infty} \left[\mathbf{A}_0 \circ (\mathbf{K}_0(x-y) \circ \mathbf{Q}_1(y) + \mathbf{K}_1(x-y,y))\right] \mathrm{e}^{s(x-y)} \boldsymbol{\phi}(y)\,\mathrm{d}y \ . \tag{B.6}$$

where $\mathbf{K}_0$, $\mathbf{K}_1$ are defined in Appendix A and $\mathbf{Q}_1$ is the relative perturbation of the population projection matrix. Substituting $\boldsymbol{\phi}(x) = \boldsymbol{\psi}_s$, and taking the inner product with $\tilde{\boldsymbol{\psi}}_s$, we have

$$\rho_1(s) = \frac{1}{sL}\int_0^L \tilde{\boldsymbol{\psi}}_s \cdot \int_{-\infty}^{\infty} \left[\mathbf{A}_0 \circ (\mathbf{K}_0(x-y) \circ \mathbf{Q}_1(y) + \mathbf{K}_1(x-y,y))\right] \mathrm{e}^{s(x-y)}\, \boldsymbol{\psi}_s \mathrm{d}y\mathrm{d}x \ . \tag{B.7}$$

To evaluate this, we introduce the change of variables

$$w = x - y \quad \text{and} \quad z = y \tag{B.8}$$

and (B.7) becomes

$$\begin{aligned}
\rho_1(s) &= \frac{1}{sL}\tilde{\boldsymbol{\psi}}_s \cdot \left[\mathbf{A}_0 \circ \int_{-\infty}^{\infty}\int_{-w}^{L-w} (\mathbf{K}_0(w) \circ \mathbf{Q}_1(z) + \mathbf{K}_1(w,z))\, \mathrm{e}^{sw}\,\mathrm{d}z\mathrm{d}w\right] \boldsymbol{\psi}_s \\
&= \frac{1}{sL}\tilde{\boldsymbol{\psi}}_s \cdot \left[\mathbf{A}_0 \circ \left(\mathbf{M}_0(s) \circ \int_{-w}^{L-w} \mathbf{Q}_1(z)\mathrm{d}z + \int_{-\infty}^{\infty}\int_{-w}^{L-w} \mathbf{K}_1(w,z)\mathrm{d}z\, \mathrm{e}^{sw}\,\mathrm{d}w\right)\right] \boldsymbol{\psi}_s \ .
\end{aligned} \tag{B.9}$$

Since $\mathbf{Q}_1(z)$ and $\mathbf{K}_1(w,z)$ are $L$-periodic in $z$ and $\int_0^L \mathbf{Q}_1(x)\mathrm{d}x = \mathbf{O}$ and $\int_0^L \mathbf{K}_1(w,x)\mathrm{d}x = \mathbf{O}$ (for all $w \in \mathbb{R}$), we have

$$\int_{-w}^{L-w} \mathbf{Q}_1(z)\mathrm{d}z = \mathbf{O} \quad \text{and} \quad \int_{-w}^{L-w} \mathbf{K}_1(w,z)\mathrm{d}z = \mathbf{O}$$

and therefore that

$$\rho_1(s) = 0 \ . \tag{B.10}$$

This means that

$$\rho(s,\epsilon) = \rho(s,0) + \mathrm{O}(\epsilon^2)$$

and

$$\begin{aligned} c(s,\epsilon) &= \frac{1}{s}\log(\rho(s,0) + \mathrm{O}(\epsilon^2)) \\ &= c(s,0) + \mathrm{O}(\epsilon^2) \ . \end{aligned} \tag{B.11}$$

This gives us that as $\epsilon \to 0^+$, $|c(s,\epsilon) - c(s,0)| < R(s)\epsilon^2$; however the $s$-dependence (a lack of *uniform convergence*) means that, on its own, this is not enough to show that the asymptotic wave-speeds $\hat{c}(\epsilon)$ and $\hat{c}(0)$ (the minima of $c(s,\epsilon)$ and $c(s,0)$) differ by $\mathrm{O}(\epsilon^2)$ in the $\epsilon \to 0^+$ limit. To do this, we need to assume that the asymptotic wave-speed is not attained in the limit as $s \to \infty$, i.e.

$$\hat{c}(0) < \lim_{s\to\infty} c(s,0) \ . \tag{B.12}$$

If this condition did not hold, then the asymptotic $t \to \infty$ limit of the solution to the linearised IDE (4) would not be smooth and would be infinite in the wave-back, so for physically realistic IDEs, we can assume (B.12). The inequality in (B.12) allows us to choose an $\eta > 0$ such that

$$\hat{c}(0) + 2\eta < \lim_{s\to\infty} c(s,0) \ , \tag{B.13}$$

so there exists an $\tilde{s}$ such that

$$c(s,0) > \hat{c}(0) + 2\eta \ \text{ for all } \ s > \tilde{s} \ . \tag{B.14}$$

We define

$$\Omega = \{(s,\epsilon) \in \mathbb{R}^2 : s \geq 0 \ \text{ and } \ \epsilon \in [0, 0.5]\} \ .$$

We then define two sets

$$\begin{aligned} \mathcal{S}_1 &= \{(s,\epsilon) \in \Omega : \epsilon = 0 \ \text{ and } \ c(s,\epsilon) \leq \hat{c}(0) + \eta\} \\ \mathcal{S}_2 &= \{(s,\epsilon) \in \Omega : c(s,\epsilon) \leq \hat{c}(0) + 2\eta\} \\ \partial\mathcal{S}_2 &= \{(s,\epsilon) \in \Omega : c(s,\epsilon) = \hat{c}(0) + 2\eta\} \ . \end{aligned}$$

$\mathcal{S}_1$ and $\mathcal{S}_2$ are closed by the continuity of $c(s,0)$. By (B.14) $\mathcal{S}_1$ and $\mathcal{S}_2$ are both bounded,

$$\mathcal{S}_1, \mathcal{S}_2 \subset [0, \tilde{s}] \times [0, 0.5]$$

so $\mathcal{S}_1$ and $\mathcal{S}_2$ are both compact, and hence $\partial\mathcal{S}_2$ is also compact. By construction, no point can be in both $\mathcal{S}_1$ and $\mathcal{S}_2$, so

$$\mathcal{S}_1 \cap \partial\mathcal{S}_2 = \emptyset \ . \tag{B.15}$$

Given (B.15) and the compactness of $\mathcal{S}_1$ and $\partial\mathcal{S}_2$, there is a minimum distance between points in $\mathcal{S}_1$ and points in $\partial\mathcal{S}_2$. This means that there exists an $\epsilon^* > 0$ such that

$$\mathcal{S}_1^* = \{(s,\epsilon) \in \Omega : \epsilon \in [0, \epsilon^*] \text{ and } c(s,\epsilon) \leq \hat{c}(0) + \eta\}$$

is a proper subset of $\mathcal{S}_2$. Since $\mathcal{S}_1^* \subset \mathcal{S}_2$, $\mathcal{S}_1^*$ is compact and $c$ is bounded on $\mathcal{S}_1^*$, and given (B.11), the function

$$A(s,\epsilon) = \begin{cases} \left(c(s,\epsilon) - c(s,0)\right)/\epsilon^2 & \text{for } \epsilon \geq 0 \\ 0 & \text{for } \epsilon = 0 \end{cases}$$

is bounded on $\mathcal{S}_1^*$, with supremum (lowest upper bound) $\tilde{A}$. Then, given that

$$c(s,\epsilon) - c(s,0) = \epsilon^2 A(s,\epsilon)$$

and that for $\epsilon$ sufficiently close to 0, $\min_{s>0} c(s,\epsilon) < \min_{s>0} c(s,0) + \eta$, so the minima is attained in $\mathcal{S}_1^*$, we have

$$\begin{aligned} |\min_{s\geq 0} c(s,\epsilon) - \min_{s\geq 0} c(s,0)| &= |\min_{s\in\mathcal{S}_1^*} c(s,\epsilon) - \min_{s\in\mathcal{S}_1^*} c(s,0)| \\ &\leq \epsilon^2 \max_{s\in\mathcal{S}_1^*} A(s,\epsilon) \\ &= \epsilon^2 \tilde{A} \ . \end{aligned}$$

So the asymptotic wave-speeds $\hat{c}(\epsilon)$ and $\hat{c}(0)$ satisfy

$$\hat{c}(\epsilon) = \hat{c}(0) + \mathrm{O}(\epsilon^2) \text{ as } \epsilon \to 0^+ \ .$$

## Appendix C. Derivation of the Second Order Term for Homogeneous Dispersal

In this section, we derive the second order approximation to the wave-speed presented in §2.2 for growth and dispersal parameters with low spatial variation. The $\mathrm{O}(\epsilon^2)$ approximation is

$$\hat{c}_2 = \min_{s>0}\left[\frac{1}{s}\log\left(\rho(s,0)+\epsilon^2\rho_2(s)\right)\right] \ . \tag{C.1}$$

We therefore need to find an expression for $\rho_2(s)$ in terms of lower order eigenvalues and eigenvectors. This is given by the $\mathrm{O}(\epsilon^2)$ terms in the eigenvalue equation (B.2)

$$(F^0-\rho(s,0))\boldsymbol{\phi}_{s,2}+(F_1^\epsilon-\rho_1(s))\boldsymbol{\phi}_{s,1}+(F_2^\epsilon-\rho_2(s))\boldsymbol{\phi}_{s,0}=0 \ .$$

Taking the inner product with $\boldsymbol{\phi}^*_{s,0}$ to eliminate the $\boldsymbol{\phi}_{s,2}$ term, noting that $\rho_{s,1}=0$ and that we have chosen the spatially constant eigenvectors $\boldsymbol{\phi}^*_{s,0}=\tilde{\boldsymbol{\psi}}_s$ and $\boldsymbol{\phi}_{s,0}=\boldsymbol{\psi}_s$ such that $\tilde{\boldsymbol{\psi}}_s\cdot\boldsymbol{\psi}_s=1$, and re-arranging, we have

$$\begin{aligned}
\rho_2(s) =& \frac{1}{L}\langle\boldsymbol{\phi}^*_{s,0}|F_1^\epsilon\boldsymbol{\phi}_{s,1}+F_2^\epsilon\boldsymbol{\phi}_{s,0}\rangle \\
=& \frac{1}{L}\tilde{\boldsymbol{\psi}}_s\cdot\int_0^L\mathbf{A}_0\circ\int_{-\infty}^{\infty}\left[\sum_{j=1}^n q_1^j(y)\mathbf{K}^j(x-y)+\mathbf{K}_0(x-y)\circ\mathbf{Q}_1(y)\right]\mathrm{e}^{s(x-y)}\boldsymbol{\phi}_{s,1}(y) \\
&+\left[\frac{1}{2}\sum_{i,j=1}^n q_1^i(y)q_1^j(y)\mathbf{K}^{i,j}(x-y)+\sum_{j=1}^n q_1^j(y)\mathbf{K}^j(x-y)\circ\mathbf{Q}_1(y)\right]\mathrm{e}^{s(x-y)}\mathrm{d}y\mathrm{d}x\,\boldsymbol{\psi}_s \ .
\end{aligned}$$

To evaluate this, we need an expression for $\boldsymbol{\phi}_{s,1}$. To do this, we again consider the $\mathrm{O}(\epsilon)$ terms in (B.2), which given that $\rho_1(s)=0$ is

$$(F^0-\rho(s,0))\boldsymbol{\phi}_{s,1}+F_1^\epsilon\boldsymbol{\phi}_{s,0}=0 \tag{C.2}$$

where $\boldsymbol{\phi}_{s,1}$ is $L$-periodic. This becomes

$$\begin{aligned}
&\int_{-\infty}^{\infty}\left[\mathbf{A}_0\circ\mathbf{K}_0(x-y)\mathrm{e}^{s(x-y)}\right]\boldsymbol{\phi}_{s,1}(y)\mathrm{d}y-\left[\mathbf{A}_0\circ\mathbf{M}_0(s)\right]\boldsymbol{\phi}_{s,1}(x) \\
&+\int_{-\infty}^{\infty}\left[\sum_{j=1}^n q_1^j(y)\mathbf{K}^j(x-y)\circ\mathbf{A}_0+\mathbf{K}_0(x-y)\circ\mathbf{A}_1(y)\right]\mathrm{e}^{s(x-y)}\boldsymbol{\psi}_s\mathrm{d}y=0 \ ,
\end{aligned} \tag{C.3}$$

with boundary conditions $\boldsymbol{\phi}_{s,1}(0)=\boldsymbol{\phi}_{s,1}(L)$. To find $\boldsymbol{\phi}_{s,1}(x)$, we take the Fourier transform of (C.3). This gives

$$\hat{\boldsymbol{\phi}}_{s,1}(\eta) = \left[\mathbf{A}_0 \circ (\mathbf{M}_0(s) - \mathbf{M}_0(s - 2\pi i\eta))\right]^{-1} \mathbf{A}_0 \circ \left[\mathbf{M}_0(s - 2\pi i\eta) \circ \hat{\mathbf{Q}}_1(\eta) + \sum_{j=1}^{n} \hat{q}^j(\eta)\mathbf{M}^j(s - 2\pi i\eta)\right] \boldsymbol{\psi}_s \ .$$

The expression for $\rho_2(s)$ is given by

$$\begin{aligned}
\rho_2(s) =& \frac{1}{L}\int_0^L \tilde{\boldsymbol{\psi}}_s \int_{-\infty}^{\infty}\int_{-\infty}^{\infty} \left[\mathbf{A}_0 \circ \left(\mathbf{M}_0(s - 2\pi i\xi) \circ \hat{\mathbf{Q}}_1(\xi - \eta) + \sum_{j=1}^{n} \hat{q}^j(\xi - \eta)\mathbf{M}^j(s - 2\pi i\xi)\right)\right] \\
&\cdot \left[\mathbf{A}_0 \circ (\mathbf{M}_0(s) - \mathbf{M}_0(s - 2\pi i\eta))\right]^{-1} \left[\mathbf{A}_0 \circ \left(\mathbf{M}_0(s - 2\pi i\eta) \circ \hat{\mathbf{Q}}_1(\eta) + \sum_{j=1}^{n} \hat{q}^j(\eta)\mathbf{M}^j(s - 2\pi i\eta)\right)\right] \\
&+ \left[\mathbf{A}_0 \left(\sum_{j=1}^{n} \hat{q}^j(\xi - \eta)\mathbf{M}^j(s - 2\pi i\xi) \circ \hat{\mathbf{Q}}_1(\eta) \right.\right. \\
&\qquad \left.\left. + \frac{1}{2}\sum_{i,j=1}^{n} \hat{q}^i(\xi - \eta)\hat{q}^j(\eta)\mathbf{M}^{i,j}(s - 2\pi i\xi)\right)\right] \mathrm{d}\eta\boldsymbol{\psi}_s \mathrm{e}^{2\pi i\xi x}\mathrm{d}\xi\mathrm{d}x \ . \qquad \text{(C.4)}
\end{aligned}$$

Since $\mathbf{Q}_1(x)$ and $q_1^j(x)$ are $L$-periodic and have spatial average $\mathbf{O}_N$ (the $N \times N$ matrix of zeros) and 0, we can write them as Fourier series with the constant terms $\mathbf{C}_0$ and $\gamma_0^j$ equal to zero,

$$\mathbf{Q}_1(x) = \sum_{n\neq 0} \mathbf{C}_n \exp\left(\frac{2\pi inx}{L}\right) \quad \text{and} \quad q_1^j(x) = \sum_{n\neq 0} \gamma_n^j \exp\left(\frac{2\pi inx}{L}\right)$$

where $\mathbf{C}_{-n} = \bar{\mathbf{C}}_n$ and $\gamma_{-n} = \bar{\gamma}_n$ for all $j$ and all $n \in \mathbb{N}$. The Fourier transforms of $\mathbf{Q}_1(x)$ and $q_1^j$ are

$$\hat{\mathbf{Q}}_1(\xi) = \sum_{n\neq 0} \mathbf{C}_n \delta\left(\xi - \frac{n}{L}\right) \quad \text{and} \quad q_1^j(x) = \sum_{n\neq 0} \gamma_n^j \delta\left(\xi - \frac{n}{L}\right) \ .$$

Substituting these into (C.4), we get

$$\begin{aligned}
\rho_2(s) =& \tilde{\boldsymbol{\psi}}_s \Bigg( \sum_{n\neq 0} \left[\mathbf{A}_0 \circ \left(\mathbf{M}_0(s) \circ \mathbf{C}_{-n} + \sum_{j=1}^{n} \gamma_{-n}^j \mathbf{M}^j(s)\right)\right] \left[\mathbf{A}_0 \circ \left(\mathbf{M}_0(s) - \mathbf{M}_0\left(s - \frac{2\pi in}{L}\right)\right)\right]^{-1} \\
&\cdot \left[\mathbf{A}_0 \circ \left(\mathbf{M}_0\left(s - \frac{2\pi in}{L}\right) \circ \mathbf{C}_n + \sum_{j=1}^{n} \gamma_n^j \mathbf{M}^j\left(s - \frac{2\pi in}{L}\right)\right)\right] \\
&+ \left[\mathbf{A}_0 \circ \left(\sum_{j=1}^{n} \gamma_{-n}^j \mathbf{M}^j(s) \circ \mathbf{C}_n + \frac{1}{2}\sum_{i,j=1}^{n} \gamma_{-n}^i \gamma_n^j \mathbf{M}^{i,j}(s)\right)\right]\Bigg) \boldsymbol{\psi}_s \ . \qquad \text{(C.5)}
\end{aligned}$$

In (C.1), we defined the second order approximation for the asymptotic wave-speed of solutions to the models with initial compact support in terms of $\rho(s, 0)$ and $\rho_2(s)$. Substituting (C.5) into (C.1), we obtain

the expressions for $\hat{c}_2$ presented in §2.2.

## Appendix D. Numerical Methods

In §3 (Examples), we compare our analytical results to simulations of the IDE. We now discuss the numerical methods used in carrying out the simulations.

We simulate the IDEs by discretising the population density function and dispersal kernels into domains of non-dimensional length $\approx 0.0015$. Since the kernels in each type of region are dependent only on the dispersal distance $x - y$, the RHS of (1) can be written as the sum of two terms, with one referring to dispersal from one region type, and the other to dispersal from the other type. Since the dispersal pattern from each type of region does not vary within that region type, the integrals are convolutions of the population density function in that region type and the dispersal kernel from that region type. Under the discretisation, the integral convolution of the population density function and dispersal kernel becomes a discrete convolution which we calculate using the Fourier convolution theorem and Fast Fourier Transform (FFT) [37]. We assume (and observe numerically) the solution will have settled into a travelling wave by the time the wave-front has reached $x = 100$. We run the simulations until $x = 200$ and use the position of the wave-front at each time-step between these two events to find the asymptotic wave-speed by fitting a linear function to the data. Numerically, we find that (after an initial transient) the wave-front maintains the same exponential shape and shifts by a fixed distance. Therefore, the observed wave-speed is independent of the final time choice, and our choice of numerical threshold for invasion $\mu$ which we thereafter take as $\mu = 0.0005$.

## References


[1] P. E. Hulme, Beyond control: wider implications for the management of biological invasions, Journal of Applied Ecology 43 (5) (2006) 835–847.

[2] D. Pimentel, R. Zuniga, D. Morrison, Update on the environmental and economic costs associated with alien-invasive species in the united states, Ecol. Econ. 52 (3) (2005) 273–288.

[3] M. Williamson, Invasions, Ecography 22 (1) (1999) 5–12.

[4] P. Pyšek, D. M. Richardson, Invasive species, environmental change and management, and health, Annu. Rev. Env. Resour. 35 (1) (2010) 25–55.

[5] P. M. Vitousek, C. M. D'Antonio, L. L. Loope, R. Westbrooks, et al., Biological invasions as global environmental change, Am. Sci. 84 (5) (1996) 468–478.

[6] Y. Zhou, M. Kot, Discrete-time growth-dispersal models with shifting species ranges, Theor. Ecol. 4 (1) (2011) 13–25.

[7] J. Bennie, J. A. Hodgson, C. R. Lawson, C. T. R. Holloway, D. B. Roy, T. Brereton, C. D. Thomas, R. J. Wilson, Range expansion through fragmented landscapes under a variable climate, Ecol. Lett. 16 (7) (2013) 921–929.

[8] J. M. Bullock, S. M. White, C. Prudhomme, C. Tansey, R. Perea, D. A. P. Hooftman, Modelling spread of British wind-dispersed plants under future wind speeds in a changing climate, J. Ecol. 100 (1) (2012) 104–115.

[9] J. M. Travis, M. Delgado, G. Bocedi, M. Baguette, K. Bartoń, D. Bonte, I. Boulangeat, J. A. Hodgson, A. Kubisch, V. Penteriani, et al., Dispersal and species responses to climate change, Oikos 122 (11) (2013) 1532–1540.

[10] M. A. Lewis, Spread rate for a nonlinear stochastic invasion, J. Math. Biol. 41 (5) (2000) 430–454.

[11] A. W. King, K. A. With, Dispersal success on spatially structured landscapes: when do spatial pattern and dispersal behavior really matter?, Ecol. Model. 147 (1) (2002) 23–39.

[12] N. Shigesada, K. Kawasaki, E. Teramoto, Traveling periodic waves in heterogeneous environments., Theor. Popul. Biol. 30 (1) (1986) 143–160.

[13] S. Dewhirst, F. Lutscher, Dispersal in heterogeneous habitats: thresholds, spatial scales, and approximate rates of spread, Ecology 90 (5) (2009) 1338–1345.

[14] M. A. Gilbert, S. M. White, J. M. Bullock, E. A. Gaffney, Spreading speeds for stage structured plant populations in fragmented landscapes, J. Theor. Biol.

[15] J. Skellam, Random dispersal in theoretical populations, Biometrika (1951) 196–218.

[16] S. A. Levin, Dispersion and population interactions, American Naturalist (1974) 207–228.

[17] M. Kot, M. A. Lewis, P. van den Driessche, Dispersal data and the spread of invading organisms, Ecology 77 (7) (1996) 2027–2042.

[18] M. G. Neubert, H. Caswell, Demography and dispersal: calculation and sensitivity analysis of invasion speed for structured populations, Ecology 81 (6) (2000) 1613–1628.

[19] J. M. Bullock, R. F. Pywell, S. J. Coulson-Phillips, Managing plant population spread: prediction and analysis using a simple model, Ecol. Appl. 18 (4) (2008) 945–953.

[20] H. Caswell, R. Lensink, M. G. Neubert, Demography and dispersal: life table response experiments for invasion speed, Ecology 84 (8) (2003) 1968–1978.

[21] M. Kot, W. M. Schaffer, Discrete-time growth-dispersal models, Math. Biosci. 80 (1) (1986) 109–136.

[22] M. G. Neubert, I. M. Parker, Projecting rates of spread for invasive species, Risk. Anal. 24 (4) (2004) 817–831.

[23] S. J. Schreiber, M. E. Ryan, Invasion speeds for structured populations in fluctuating environments, Theor. Ecol. 4 (4) (2011) 423–434.

[24] O. Skarpaas, K. Shea, Dispersal patterns, dispersal mechanisms, and invasion wave speeds for invasive thistles, Am. Nat. 170 (3) (2007) 421–430.

[25] J. M. Travis, C. M. Harris, K. J. Park, J. M. Bullock, Improving prediction and management of range expansions by combining analytical and individual-based modelling approaches, Methods in Ecology and Evolution 2 (5) (2011) 477–488.

[26] K. Kawasaki, N. Shigesada, An integrodifference model for biological invasions in a periodically fragmented environment, Jpn. J. Ind. Appl. Math. 24 (1) (2007) 3–15.

[27] P. Jurena, S. Archer, Woody plant establishment and spatial heterogeneity in grasslands, Ecology 84 (4) (2003) 907–919.

[28] R. Miller, J. Ver Hoef, N. Fowler, Spatial heterogeneity in eight central texas grasslands, Journal of Ecology (1995) 919–928.

[29] M. Janišová, K. Hegedüšová, P. Král', I. Škodová, Ecology and distribution of *tephroseris longifolia* subsp.*moravica* in relation to environmental variation at a micro-scale, Biologia 67 (1) (2012) 97–109.

[30] H. F. Weinberger, On spreading speeds and traveling waves for growth and migration models in a periodic habitat, J. Math. Biol. 45 (6) (2002) 511–548.

[31] J. R. Poulsen, C. W. Osenberg, C. J. Clark, D. J. Levey, B. M. Bolker, Plants as reef fish: fitting the functional form of seedling recruitment, Am. Nat. 170 (2) (2007) 167–183.

[32] M. Kot, Discrete-time travelling waves: ecological examples, J. Math. Biol. 30 (4) (1992) 413–436.

[33] R. E. Snyder, How demographic stochasticity can slow biological invasions, Ecology 84 (5) (2003) 1333–1339.

[34] J. A. Metz, D. Mollison, F. Van Den Bosch, The dynamics of invasion waves, The geometry of ecological interactions: simplifying spatial complexity. Cambridge University Press, Cambridge (2000) 482–512.

[35] P. Skelsey, K. A. Garrett, et al., Why dispersal should be maximized at intermediate scales of heterogeneity, Theor. Ecol. 1–9.

[36] J. Clobert, M. Baguette, T. G. Benton, J. M. Bullock, Dispersal ecology and evolution, 1st Edition, Oxford University Press, 2012.

[37] M. Andersen, Properties of some density-dependent integrodifference equation population models, Math. Biosci. 104 (1) (1991) 135–157.